Russian Chemical Reviews **68** (4) 299 – 316 (1999) © 1999 Russian Academy of Sciences and Turpion Ltd

UDC 548.736

Electron density and traditional structural chemistry of silicates

E L Belokoneva

Contents

I.	Introduction	299
II.	Orthosilicates	300
III.	Ring silicates	303
IV.	Chain and band silicates	308
V.	Sheet silicates	308
VI.	Framework silicates	310
VII.	Quantum-chemical calculations of selected framework structures	313
VIII.	Determination of charges on atoms in silicates	313
IX.	Conclusion	314

Abstract. New results of studies on the electron density of silicates are considered in accordance with the traditional structural classification. Precision X-ray diffraction data and results of structure refinement based on high-angle and multipole models are discussed. Bonded radii, charges on atoms and bond ionicities in Si, Al, B and Be tetrahedra are estimated from the deformation electron density maps in relation to the electronic structures of the atoms and their electronegativities. New possibilities for the solution of problems of isomorphism, for investigations on hydrogen bonds and for the classification are demonstrated. It is noted that the electron density distributions allow one to consider fundamentals of traditional structural chemistry of silicates on the electronic level. For selected compounds, the results of experimental studies of the electron density and of quantum-chemical calculations are compared. The bibliography includes 97 references.

I. Introduction

Silicates are substances whose structures contain different combinations of silicon-oxygen tetrahedra as the major anionic components. Their negative charges are compensated for by charges of cations bulkier than silicon (for example, by magnesium, iron, calcium, sodium or potassium cations). Silicates belong to rock-forming minerals, which account for 90% of the Earth's crust. Virtually all elements of the Periodic table ranging from hydrogen to uranium and transuranium elements are the components of these minerals. Many silicates are mined and used as sources of raw materials.

The discovery of X-ray diffraction and the development of a fundamentally new method for studying compounds, *viz*., X-ray diffraction analysis, have had a crucial effect on the studies of silicate structures. Before this method had been developed, numerous 'salts of polysilicic acids,' which are virtually insoluble in strong acids, had presented a puzzle for chemists. In the first studies performed in the mid-1920s, the structures of garnet (the first silicate), quartz, olivine, sphene, zircon, diopside, topaz, phenakite, willemite, beryl, vesuvianite, benitoite, hypersthene, staurolite, hemimorphite and thortveitite were solved.[1,2] Abundant data on silicate structures have now been accumulated. Russian scientists, namely, Academician N V Belov and his followers, have contributed significantly to the development of the notion of silicate structures.[3]

The advent of automated diffractometers and programme packages for special data processing marked the beginning of precision X-ray diffraction studies. The review by Tsirelson [4] was the first Russian publication in which the current state of precision X-ray diffraction investigations and the modern notion of the electron density distribution in crystals have been covered most comprehensively. Examples of structural studies of organic and inorganic compounds, including silicates, were also reported in the cited review. Presently, studies on the electron density are among intensively developing lines of investigation in the structural chemistry. The principles and methods of investigations of the electron density are considered in detail in the monographs.[4–7]

Classical (traditional) investigations in the field of structural chemistry of silicates were most completely surveyed in the monograph by Liebau.[8] In this monograph, precision X-ray diffraction studies of silicates were briefly considered and the deformation electron density maps for orthoenstatite and coesite were presented. However, the currently available factual data are substantially more abundant.

The publications by Tsirelson *et al*.,[9,10] can be considered as the first reviews devoted to the studies on the electron density of silicates. In the latter review, the major concepts, including principles of interpretation of electron density maps, were reported. A total of about 20 structures were discussed in these publications.

The present review surveys the results of studies on the electron density distribution in silicates published in recent years. Taking into account new data, crystal-chemical notions, such as the bond ionicity, the effective radius and the charge on the atom, as well as principles of the classification of silicate structures, which are compared with the classical views, are considered.[8] For selected structures, the results of experimental studies on the electron density are compared with the results of quantum-chemical calculations.

E L Belokoneva Department of Geology, M V Lomonosov Moscow State University, Leninskie gory, 119899 Moscow, Russian Federation.
Fax (7-095) 932 88 89. Tel. (7-095) 939 49 26. E-mail: elbel@geol.msu.ru

Received 11 September 1998
Uspekhi Khimii **68** (4) 331 – 348 (1999); translated by T N Safonova

In the analysis of the results of investigations of silicate structures by the precision X-ray diffraction method, particular attention is given to the chemical bonds (especially, to those in silicon–oxygen tetrahedra). The data on these bonds can be obtained from electron density maps. The experimental electron density maps constructed with the use of the known procedures [4–7] revealed regions of concentration of the electron density which were identified with overlapping orbitals. The silicon atom in the $[SiO_4]$ tetrahedron possesses four equivalent sp^3-hybrid orbitals corresponding to single covalent σ-bonds.[11,12] In silicates, the experimental average SiO distance is shorter than that calculated with the use of Shomaker–Stevenson' equation taking into account the covalent radii of the silicon and oxygen atoms for the single bond. Cruickshank suggested [11] that the remaining *p*-orbitals of the oxygen atoms overlap with the *d*-orbitals of the silicon atoms to form additional π-bonds, which impart a somewhat double character to Si—O interactions. This fact was noted by Liebau [8] and Tsirelson *et al.*[10]

Most studies on the chemical bonds in silicates involved calculations of deformation electron density distribution maps on the basis of an independent spherical-atom model (IAM), which is refined based on high-angle reflections (high-angle refinement), and the determination of the deformation component of the density ($\delta\rho$) responsible for the chemical bond with the use of difference Fourier series [4–7]

$$\delta\rho(\mathbf{r}) = \frac{1}{V}\sum [F_{\exp}(\mathbf{s}) - F_{\mathrm{IAM}}(s)]\exp(-2\pi i\mathbf{sr}),$$

where V is the unit cell volume, $F_{\exp}$ is the experimental structure amplitude, F_{IAM} is the calculated structure amplitude of the independent spherical model, **s** is the scattering vector of the reciprocal lattice, which describes the reflection of the *hkl* node, and **r** is the radius vector.

Therefore, the deformation electron density $\delta\rho$ characterises the electron density redistribution upon the involvement of atoms in chemical bonding.

The method of the multipole analysis of the electron density differs fundamentally from that of the high-angle refinement.[4–7,10,13,14] The atomic scattering factor can be calculated from the following formula:

$$\mathrm{f}(q) = P_{\mathrm{c}}\mathrm{f}_{\mathrm{c}}(q) + P_{\mathrm{v}}\mathrm{f}_{\mathrm{v}}\left(\frac{q}{æ}\right),$$

where P_{c} and P_{v} are population coefficients of the core and valence shells, respectively, and $\mathrm{f}_{\mathrm{c}}(q)$ and $\mathrm{f}_{\mathrm{v}}(q/æ)$ are their scattering factors. The parameter æ accounts for contraction or expansion of the valence shell of the atom. Chemical bonding leads to deviation from the spherical symmetry of the valence shell. However, this deviation is relatively small and can be described by the low-order expansion of the electron density in terms of nucleus-centred angular harmonics. For this purpose, different models are used, those suggested by Hansen and Coppens [13] and by Stewart and Spackman [14] are most generally employed. As an example let us consider the equation for the electron density suggested by Hansen and Coppens

$$\rho_{\mathrm{a}}(\mathbf{r}) = P_{\mathrm{c}}\rho_{\mathrm{c}}(r) + P_{\mathrm{v}}æ'^3\rho_{\mathrm{v}}(æ'r) + \sum_{l=0}^{4} æ''^3 R_l(æ''r)\sum_{m=0}^{l} P_{lm}y_{lm}\left(\frac{\mathbf{r}}{r}\right),$$

where **r** is the radius vector, P_{c}, P_{v} and P_{lm} are the population coefficients of the core, valence and deformation components, respectively, æ′ and æ″ are the expansion–contraction parameters of the valence and multipole shells, respectively, R_l are the radial functions and y_{lm} are spherical harmonics (up to the fourth order); $r = |\mathbf{r}|$.

The atom is represented as the sum of the core, valence and deformation (multipole) electron densities. The population coefficients of the valence and multipole terms, the parameters of the radial functions P_{lm} and the æ′ and æ″ parameters are refined by the least-squares method. The refinement is performed until the closest agreement between the calculated and experimental structure factors is achieved.

Precision calculations of silicate structures are carried out with the use of different programme packages, which allow one to process experimental data, to perform the refinement within the framework of a particular model and to construct sections of the electron density distribution passing through the interacting atoms. The following programmes can serve as examples: LINUS and its modified version EARTH,[15] RADIEL,[16] CRYLSQ,[17] FOURR,[18] SADIAN90,[19] MINEXTL,[20] *etc.* The improved programme packages MOLLY [13] and VALRAY [14] are most generally used for the multipole refinement. Presently, the XD programme package,[21] which involves modern investigation techniques, including topological analysis of the electron density, provides the greatest scope.

In the present review, most attention is concentrated on the results of high-angle refinement because only five examples of multipole refinement are known for silicates. The structures are considered in accordance with the degree of condensation of tetrahedra in the $[Si_nO_m]^{q-}$ anionic silicon–oxygen motif. In crystal chemistry, this motif is also referred to as a radical. This consideration corresponds to the classical mineralogical classification.[22–25]

II. Orthosilicates

Orthosilicates involve structures consisting of isolated (island) silicon-oxygen *ortho* groups. Natural and synthetic orthosilicates, *viz.*, Mg-, Fe-, Ni-, Co- and Mn-olivines,[26–30] Fe-, Co- and Ni-spinels,[31,32] phenakite,[33,34] euclase,[35] eulytine,[36] topaz [37] and sphene,[38] were studied by precision methods.

1. Topaz

A specimen of natural topaz from the Volyn' deposit (Ukraine) was studied.[37] Intensities of reflection were measured within four octants of the reciprocal space related by a $\bar{4}$ axis. The principal crystallographic characteristics and conditions of the X-ray diffraction study are given in Table 1. Calculations were carried out using the MINEXTL programme. The extraordinarily high extinction was taken properly into account using the Zachariasen algorithm. An independent atomic model was obtained in the high-angle refinement, the *c* coefficient in the weighting scheme being varied:

$$w_{\mathrm{s}} = [\sigma^2 + (cF^2)]^{-1},$$

where σ is the standard deviation and F is the structure factor. The correctness of the choice of the weighting scheme and of the determination of the scale factor was checked using Abrahams–

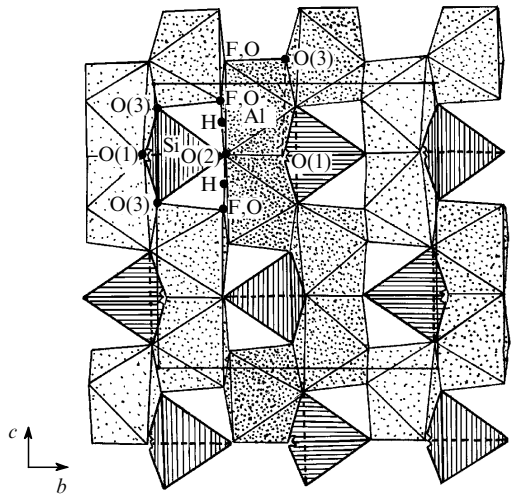


Figure 1. Structure of topaz.

Table 1. Crystallographic characteristics and conditions of X-ray diffraction studies of silicates.

Mineral	Space group	Unit cell parameters				*A*	*B*	*C*	Refinement parameters		
		a /Å	*b* /Å	*c* /Å	*β* /deg				*R* (%)	R_w (%)	*S*
Topaz $Al_2[SiO_4]F_2$	*Pbnm*	4.6511(8)	8.802(1)	8.402(1)	–	4694	1356	715	0.99	1.16	1.03
Sphene $CaTiO[SiO_4]$	$P2_1/a$	7.061(1)	8.7165(9)	6.5603(9)	113.84(1)	6924	3043	2445	1.63	2.81	1.18
Beryl $Be_3Al_2[Si_6O_{18}]\cdot H_2O$	*P6/mcc*	9.222(3)	–	9.204(1)	–	4671	752	338	0.73	0.79	1.02
Cordierite $Mg_2Al_3Al[Si_5O_{18}]\cdot H_2O$	*Cccm*	17.155(5)	9.777(4)	9.339(4)	–	6324	1982	1058	1.18	1.19	1.02
Dioptase $Cu_6[Si_6O_{18}]\cdot 6H_2O$	$R\bar{3}$	14.597(2)	–	7.796(1)	–	3878	1593	625	1.90	2.00	0.87
Tourmaline $NaMg_3B_3Al_6Si_6O_{27}(OH)_4$	*R3m*	15.890(8)	–	7.129(3)	–	7383	1389	458	2.36	3.48	1.19
Datolite $CaBSiO_4(OH)$	$P2_1/a$	9.646(6)	7.620(4)	4.839(3)	90.14(5)	6018	2584	1250	1.28	1.33	1.00
Coesite SiO_2	*C2/c*	7.1367(4)	12.369(1)	7.1742(5)	–	7253	1716	1716	1.25	1.23	1.35
Danburite $CaB_2Si_2O_8$	*Pnam*	8.0456(7)	8.7629(4)	7.7341(7)	–	16243	3315	3315	3.46	5.80	0.87
Natrolite	*Fdd2*	18.293(1)	18.641(1)	6.5871(6)	–	13920	3471	1856	0.9	0.8	1.40
$Na_2Al_2Si_3O_{10}\cdot 2H_2O$		18.288(2)	18.631(2)	6.583(1)	–	8250	5191	1961	2.16	2.20	1.27
Phenakite Be_2SiO_4	$R\bar{3}$	12.485(3)	–	8.264(3)	–	3935	1270	324	1.52	1.62	0.978
		12.472(2)	–	8.251(1)	–	11700	1053	1053	1.84	1.77	1.834

Note. Notation adopted: *A* is the number of measured reflections; *B* is the number of independent reflections; *C* is the number of reflections used in the high-angle or multipole refinement.

Keve's test.[39] The refined real structural formula of the specimen is $Al_2[SiO_4](F_{0.95}OH_{0.05})$; its structure is shown in Fig. 1.

The deformation density distribution in the sections of the $[SiO_4]$ tetrahedron is in agreement with the concept of the presence of sp^3-hybridisation and σ-bonds. The map calculated for the O(1)–Si–O(3) section in topaz based on the experimental results and the map calculated for O–Si–O in the H_4SiO_4 molecule by the quantum-chemical method [40] are similar. Thus the $\delta\rho$ maxima have close values (0.40 and 0.35 e Å^3 for topaz and O–Si–O, respectively) and these maxima in both maps are shifted toward the more negative oxygen atom (Fig. 2 *a,b*).† In other orthosilicates (olivine, spinel, euclase and phenakite), the values of the corresponding maxima are in the range of 0.2–0.4 e Å^{-3}. Calculations of the error maps demonstrated that these errors in the chemical bond region were 0.05 e Å^{-3}. A comparison of the electron density distributions at the faces of the tetrahedra in topaz and olivine also demonstrates that they are basically similar. However, a slight spread in values of the maxima in the σ-bonds is observed. Note that topaz is characterised by a four-layer close packing, while olivine is described by a two-layer close packing.

The average Si–O distances in the tetrahedra are diminished as the degree of their condensation increases.[8, 25, 41] This is associated with the electrostatic interactions of the atoms. In the cases that electropositive cations (potassium, sodium, magnesium or calcium) in the structure dominate over electronegative silicon ions, simple anionic motifs, in which oxygen atoms adopt high coordination numbers and the Si–O bonds are elongated, are realised.[25] The potassium, sodium, magnesium and calcium cations rather readily donate electrons to the oxygen atoms, thus increasing their effective charges upon chemical bonding so that the ability of oxygen atoms to ionise silicon atoms decreases.[42] Hence, the second coordination sphere of the silicon atom has a determining effect on the electron density distribution in the silicon–oxygen tetrahedra in orthosilicates. In topaz and olivine, this sphere is formed by the Al atoms or by the Fe and Mg atoms, respectively. These atoms occupy octahedral cavities of the close packings in different fashions. The influence of the cations of the second coordination sphere is most clearly manifested in the electron density map as the splitting of the peak at the oxygen atom due to interactions between the oxygen atom and two aluminium atoms located to its right and left above the closely

† In the figures, which present the electron density distributions, the maps are contoured as follows: the solid lines indicate positive values of $\delta\rho$; the dash-and-dot lines indicate the zero level; the dashed lines indicate negative values of $\delta\rho$.

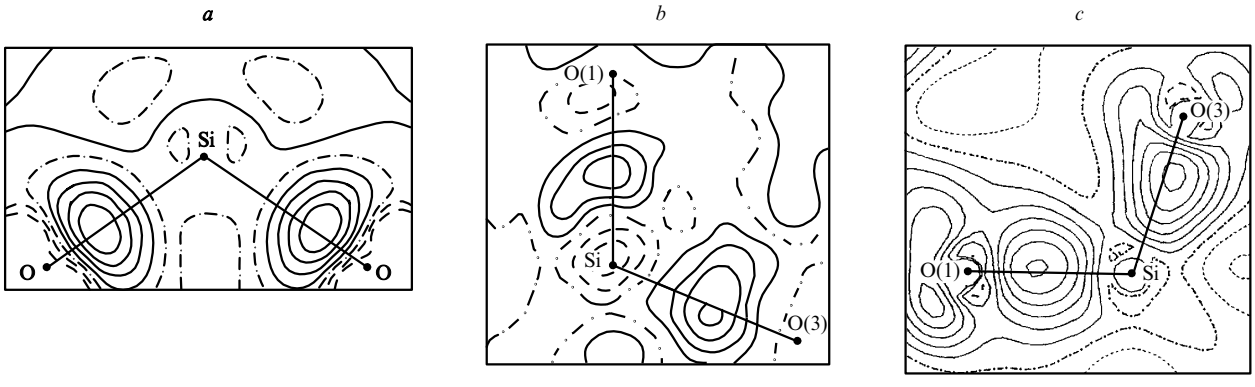


Figure 2. The electron density distribution in the H_2SiO_4 molecule (*a*) and in topaz (*b*, *c*); (*a*) the deformation density calculated for the SiO_2 group in the H_4SiO_4 molecule, the map is contoured at intervals of 0.07 e Å^{-3} (see Ref. 40); (*b*) the experimental deformation density in the O(1)–Si–O(3) section; (*c*) the static deformation density in the O(1)–Si–O(3) section, the maps are contoured at intervals of 0.1 e Å^{-3}.

packed layer. The sections through the layers of the close packing indicate that the electron density of the oxygen atoms is shifted along the bond toward the occupied octahedral (Al) and tetrahedral (Si) holes.

The multipole refinement of the $\rho(\mathbf{r})$ function [43] based on the same experimental results as those used in another study,[37] confirmed the principal characteristic features of the electron density distribution and the crystal-chemical conclusions made previously. Calculations were carried out with the use of the MOLDOS96 and SALDOS97 programmes.[44] The characteristics of the refinement ($R = 0.91\%$, $R_w = 1.1\%$, $S = 1.13$) were improved compared to the data given in Table 1.

The calculated and experimental deformation density maps for the silicon–oxygen tetrahedron are virtually identical (see Fig. 2 *a,c*). Analysis of the static deformation density maps calculated based on the results of multipole refinement most clearly revealed the shift of the electron density of the oxygen atoms in the close packed layer toward the occupied holes (Fig. 3). The splitting of the maximum at the O(2) atom toward two aluminium atoms was also reproduced.

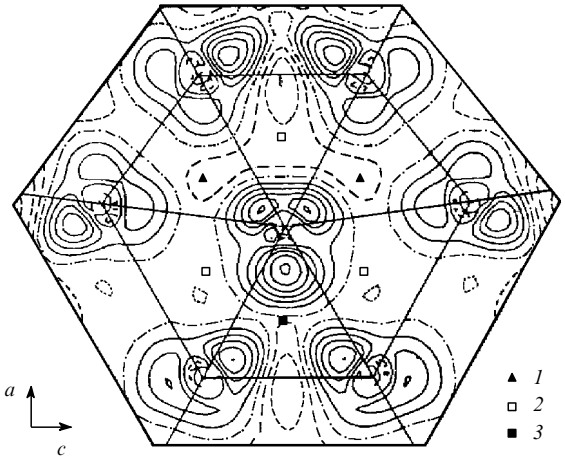


Figure 3. The static deformation density distribution in the section of topaz passing though close packed layers of O(1) (in the centre) and O(3) atoms (at the vertices of the internal hexagon); the map is contoured at intervals of 0.1 e Å^{-3}. The positions of the atoms: (*1*) Al in octahedral holes above the close packed layer; (*2*) unoccupied octahedral holes below the close packed layer; (*3*) Si in tetrahedral holes.

The charges on the atoms in topaz were estimated on the basis of the results of determination of population coefficients of valence shells.[43] In this work, considerable attention has been given to the topological analysis of the electron density, which is an intensively developing modern method [6,7] (this method is not considered in the present review). Note however that according to Bader's theory [4,6] chemical interactions in the silicon–oxygen tetrahedron are interpreted to a greater degree as ionic (*i.e.*, as interactions of atoms with closed electron shells) rather than as covalent interactions. This is inconsistent with the experimental and theoretical data obtained to date.

2. Sphene

A synthetic crystal of sphene $CaTiO[SiO_4]$ grown by Czochralski's method (Fig. 4) was investigated.[38] This mineral possesses antiferroelectric properties. The investigators attempted to relate these properties to the electronic structure. The conditions of the X-ray diffraction study are given in Table 1. Calculations were carried out with the use of the MINEXTL programme package.

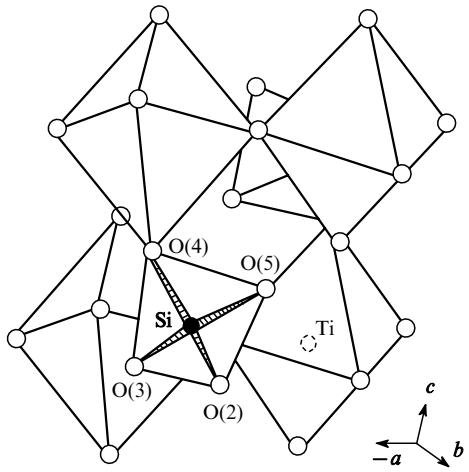


Figure 4. Structure of sphene.[38]

The distances in the silicon–oxygen tetrahedra in sphene and topaz (Table 2) are close to each other and are larger than those in other silicates containing condensed anionic groups. The deformation electron density distribution corresponds to four σ-bonds (sp^3-p) with maxima of 0.2–0.4 e Å^{-3}. The effect of the second coordination sphere on the electron density in the isolated $[SiO_4]$ tetrahedron can be judged from the difference in the values of peaks in the bonds between the silicon atom and the oxygen atoms belonging to the edge shared by Ti octahedra in a column and to the edge shared by Ti octahedra of two different columns (Fig. 5 *a*). An electron-density 'bridge' (0.2 e Å^{-3}) is clearly seen on the edge. This bridge can be interpreted as the manifestation of a somewhat double character of the bridging Si–O bonds in this structure. The error of $\delta\rho$ in the chemical-bond region was 0.2 e Å^{-3}.

The asymmetrical deformation density distribution was observed in the Ti octahedron, the density being concentrated at the shortened titanyl Ti–O(1) bond [1.7594(7) Å; Fig. 5 *b*], which

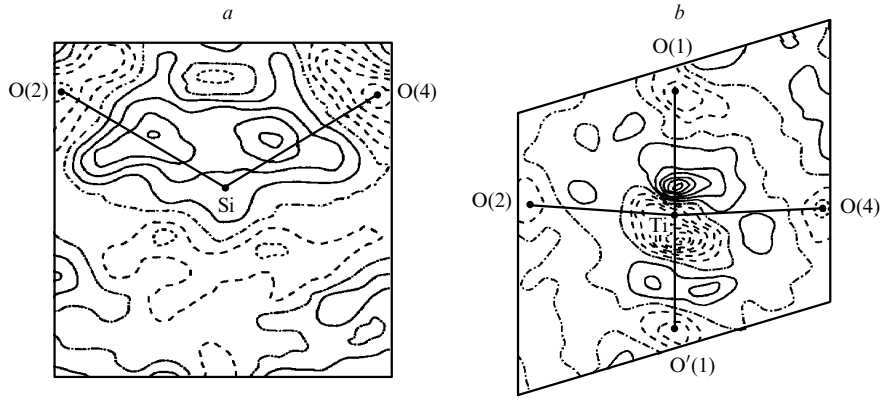


Figure 5. The experimental deformation density distribution in the section of the Si tetrahedron (*a*) and Ti octahedron (*b*) in sphene;[38] (*a*) the O(2)–Si–O(4) section, the map is contoured at intervals of 0.05 e Å^{-3}; (*b*) the O(2)–Ti–O(4)–O(1)–O′(1) section, the map is contoured at intervals of 0.1 e Å^{-3}.

Table 2. Interatomic distances in the tetrahedra of silicate structures determined in precision X-ray diffraction studies.

Tetrahedron	Atoms	Distance /Å	Tetrahedron	Atoms	Distance /Å	Tetrahedron	Atoms	Distance /Å
Topaz			Dioptase			Danburite		
$[SiO_4]$	Si – O(1)	1.636(1)		Si – O(2)	1.596(2)	$[BeO_4]$	B – O(1)	1.479(1)
	Si – O(2)	1.646(1)		Si – O(3)	1.528(2)		B – O(2)	1.500(1)
	Si – O(3)	1.641(1)×2			**1.598**		B – O(3)	1.463(1)
		1.641	Tourmaline				B – O(5)	1.454(1)
Sphene			$[SiO_4]$	Si – O(4)	1.626(3)			**1.474**
$[SiO_4]$	Si – O(2)	1.6410(5)		Si – O(5)	1.639(3)	Natrolite		
	Si – O(3)	1.6418(5)		Si – O(6)	1.607(2)	$[Si(1)O_4]$	Si(1) – O(1)	1.6056(8)×2
	Si – O(4)	1.6401(7)		Si – O(7)	1.615(2)		Si(1) – O(5)	1.6310(9)×2
	Si – O(5)	1.6429(6)			**1.622**			**1.616**
		1.6415	Datolite			$[Si(2)O_4]$	Si(2) – O(2)	1.6193(6)
Beryl			$[SiO_4]$	Si – O(1)	1.575(4)		Si(2) – O(3)	1.6121(7)
$[SiO_4]$	Si – O(1)	1.623(1)		Si – O(2)	1.649(5)		Si(2) – O(4)	1.6133(8)
	Si – O(1′)	1.595(1)		Si – O(3)	1.656(5)		Si(2) – O(5)	1.6368(9)
	Si – O(2)	1.600(1)×2		Si – O(4)	1.660(4)			**1.6204**
		1.610			**1.635**	$[Al(1)O_4]$	Al(1) – O(1)	1.7371(9)
$[BeO_4]$	Be – O	1.657×4	$[BO_4]$	B – O(2)	1.484(5)		Al(1) – O(2)	1.7457(6)
Cordierite				B – O(3)	1.479(6)		Al(1) – O(3)	1.7344(6)
$[Si(1)O_4]$	Si(1) – O(2)	1.630×4		B – O(4)	1.470(4)		Al(1) – O(4)	1.7430(8)
$[Si(2)O_4]$	Si(2) – O(1)	1.638(0)×2		B – O(5)	1.497(3)			**1.7400**
	Si(2) – O(5)	1.587(1)			**1.483**	Phenakite		
	Si(2) – O(6)	1.609(1)	Coesite			$[Si(1)O_4]$	Si(1) – O(1)	1.631(2)
		1.618	$[Si(1)O_4]$	Si(1) – O(1)	1.595(1)		Si(1) – O(2)	1.630(2)
$[Si(3)O_4]$	Si(3) – O(3)	1.640(0)×2		Si(1) – O(3)	1.613(2)		Si(1) – O(3)	1.631(1)
	Si(3) – O(4)	1.574(1)		Si(1) – O(4)	1.611(4)		Si(1) – O(4)	1.637(1)
	Si(3) – O(6)	1.616(1)		Si(1) – O(5)	1.621(1)			**1.632**
		1.618			**1.610**	$[Be(1)O_4]$	Be(1) – O(1)	1.638(2)
$[Al(1)O_4]$	Al(1) – O(2)	1.766(0)×2	$[Si(2)O_4]$	Si(2) – O(2)	1.6118(3)		Be(1) – O(2)	1.641(2)
	Al(1) – O(4)	1.710(1)		Si(2) – O(3)	1.6140(6)		Be(1) – O(4)	1.659(2)
	Al(1) – O(5)	1.713(1)		Si(2) – O(4)	1.605(4)		Be(1) – O(4′)	1.650(3)
		1.741		Si(2) – O(5)	1.6186(7)			**1.647**
$[Al(2)O_4]$	Al(2) – O(1)	1.758(0)×2			**1.6124**	$[Be(2)O_4]$	Be(2) – O(1)	1.647(2)
	Al(2) – O(3)	1.755(0)×2	Danburite				Be(2) – O(2)	1.645(2)
		1.756	$[SiO_4]$	Si – O(1)	1.6187(8)		Be(2) – O(3)	1.659(2)
Dioptase				Si – O(2)	1.6238(8)		Be(2) – O(3′)	1.643(3)
$[SiO_4]$	Si – O(1)	1.615(2)		Si – O(3)	1.6150(8)			**1.649**
	Si – O(1′)	1.651(2)		Si – O(4)	1.6158(8)			
					1.618			

Note. Average values are given in boldface type.

is apparently responsible for the appearance of the electric moment in the structure. The difference in the bond lengths and, correspondingly, in the charges on these bonds is typical of many compounds containing titanium atoms. For example, the titanyl bond in $KTiOPO_4$, which exhibits nonlinear-optical properties, is often considered as a double bond. This conclusion was made on the basis of calculations of the valence forces of the bond. The antiferromagnetic properties of sphene may result from the antiparallel distribution of the anisotropy of Ti – O interactions.

The radii of the best separation or the bonding radii were estimated from the full electron density maps.[45] It was noted that these radii were distributed over two pairs of the bonds of the silicon atom (0.85 and 0.49 Å; the average value is 0.67 Å). The estimation of the radius of the oxygen atom from the corresponding bonds in sphene gave the values 0.78 and 1.17 Å (the average value is 0.98 Å). The latter value differs only slightly from the corresponding values reported for coesite and stishovite[41] (0.95 and 1.05 Å, respectively).

III. Ring silicates

Ring silicates are minerals the structures of which consist of silicon – oxygen tetrahedra arranged in rings. This group of silicates considered previously[9, 10] was supplemented with a large number of new subjects.

1. Beryl

A specimen of natural beryl which was virtually free of impurities with the real structural formula $Na_{0.04}Be_{2.98}Al_2[Si_6O_{18}]\cdot 0.3H_2O$ (Fig. 6) was studied.[9, 10] Investigation of the electron density

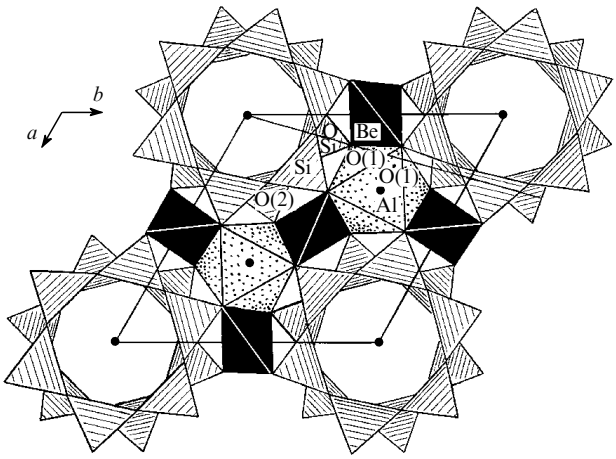


Figure 6. Structure of beryl.[46]

distribution made it possible to characterise chemical bonds in the six-membered $[Si_6O_{18}]$ ring, the Be tetrahedron, the Al octahedron and in the structure as a whole.[46,47] Actually, a group of beryls (exhibiting microisomorphism) containing various impurities of *3d* elements (Fe, Co, Cu and Cr) which impart a typical colour to the crystals (*viz*., aquamarine is pale-blue, emerald is green, *etc*.) was studied. The results of studies of microisomorphism were considered in detail.[48] Chromophore impurity ions occupy the positions of Al in octahedra (Fe, Co or Cr) or Be in tetrahedra (Cu) rather than interstitial sites as suggested previously. In addition to *3d* elements, beryl structures contain small impurities of sodium atoms and water molecules. Their positions were determined as 2(*b*) (0 0 0) for the Na atom and 2(*a*) (0 0 1/4) for the oxygen atom of the water molecule. On the basis of the arrangement of the $\delta\rho$ maxima (0.4 e Å^{-3}) in the electron density maps, the planes of the water molecules were found to be oriented horizontally (parallel to the *ab* plane), their own twofold axes being perpendicular to the principal sixfold axis (Fig. 7 *a*). This distribution was characterised on the assumption that molecules are statistically disordered about the sixfold axis. The electron density distributions in all horizontal and vertical (parallel to the *c* axis) sections for isomorphous modifications of beryls steadily reproduced the hydrogen bond pattern. The errors of the maps were 0.02 – 0.05 e Å^{-3}.

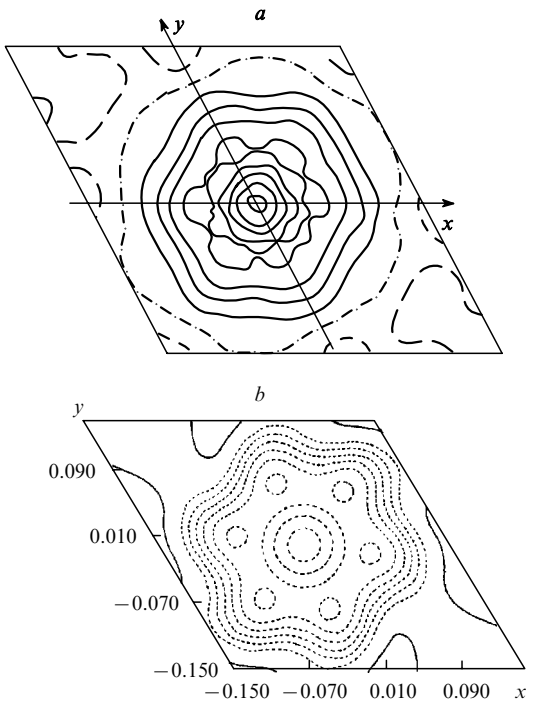


Figure 7. The experimental deformation density distribution in the section of beryl passing through the oxygen atom of the water molecule, $z = 0.25$ (*a*) and the difference Fourier map (neutron diffraction data, 30 K), $z = 0.317$ (*b*).[49]

The horizontal orientation of the water molecules corresponds to one of two models of beryl structures proposed for interpreting their IR spectra. The model that assumes the vertical orientation of the planes of the water molecules was not confirmed by our investigations. Neutron diffraction studies [49,50] of the structure of beryl confirmed the horizontal orientation of the water molecules established previously [46,47] (Fig. 7 *b*). The statistical disorder was assumed. However, the peaks around the position 2(*a*) (0 0 1/4) were misinterpreted as those possessing the mirror symmetry: in the space group of beryl (see Table 1) this position has the point symmetry 622, while the point symmetry 6/*m* is typical of position 2(*b*) (0 0 0) (Na atoms). The maxima on the sixfold axis in the vicinity of the site (0 0 1/4) are apparently due to lone electron pairs of the water molecules. Other orientations of the water molecules in beryls are also not ruled out.[49,50] Unfortunately, the vertical sections in which the positions of the hydrogen atom under consideration could be clearly seen were not presented.

2. Cordierite

The mineral cordierite $Mg_2Al_3AlSi_5O_{18}$ is structurally similar to beryl although its symmetry is lower (see Table 1).[51] The high-temperature modification of cordierite with the beryl structure has long been known.[52] Both minerals consist of six-membered rings of tetrahedra occupied by silicon atoms in beryl and by silicon and aluminium atoms in cordierite. Additional Be tetrahedra in beryl and Si and Al tetrahedra in cordierite are linked with the tetrahedra of rings *via* shared vertices to form open-work tetrahedral frameworks with bulky cavities filled by Na atoms and H_2O and CO_2 molecules (Fig. 8). Currently, cordierite in the form of ceramics is considered as an adsorbent of harmful Zn-containing exhausts of motor transport.[53] In this connection, the problem of incorporation of impurities into this zeolite-type framework is under investigation. In addition to studies on microisomorphism of *3d* elements in beryls,[48] incorporation of Cu^+ and Cu^{2+} ions into cordierites was examined by the Rietveld method.[54] The electron density maximum at the site (0 0 0), which is analogous to that observed in beryl, was attributed to the incorporation of copper atoms.

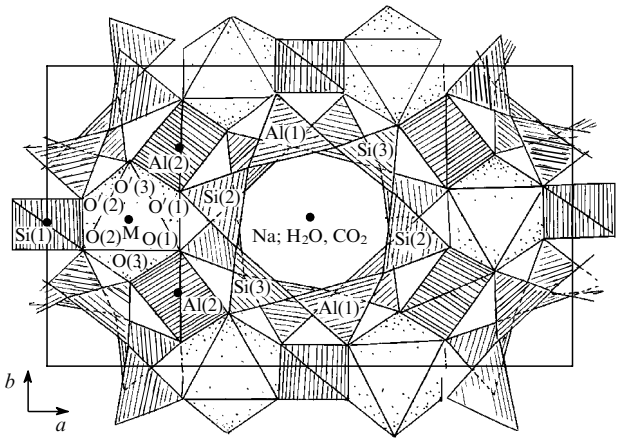


Figure 8. Structure of cordierite.[51] M is the (Mg, Fe, Mn) octahedron.

Precision investigation of a single crystal of cordierite (a natural specimen from the Tuva deposit) demonstrated that the crystal-chemical formula of the mineral taking into account microisomorphism was $Na_{0.04}(Mg_{1.13}Fe_{0.78}Mn_{0.05})Al_2Si.[Al_2Si_4O_{18}]\cdot 0.02H_2O\cdot 0.06CO_2$. X-ray diffraction data were collected within a hemisphere of the reciprocal space. Calculations were carried out with the use of the MINEXTL programme. An iron impurity in Mg octahedra was detected. The site (0 0 0) of the Na atoms is identical with that in beryl. It is worthy of note that this position is too 'bulky' for copper atoms, which should cause the impurity atom to displace from the centre of the cavity. It seems more likely that copper and zinc impurity atoms in the structure of cordierite occupy positions of 'non-ring' tetrahedra or Mn octahedra. Water molecules together with CO_2 occupy the position (0 0 1/4) in a channel identical with that in the above-considered structure of beryl.

It is of most interest to compare the electron density distributions and to reveal the difference in the chemical bonds when different atoms fill the same structural units. The deformation density distributions in the $[Si_6O_{18}]$ and $[Al_2Si_4O_{18}]$ rings in beryl and cordierite, respectively, are shown in Fig. 9 *a,b*. In the low-temperature modification of cordierite, Al and Si atoms are distributed over tetrahedral positions in an orderly fashion (see

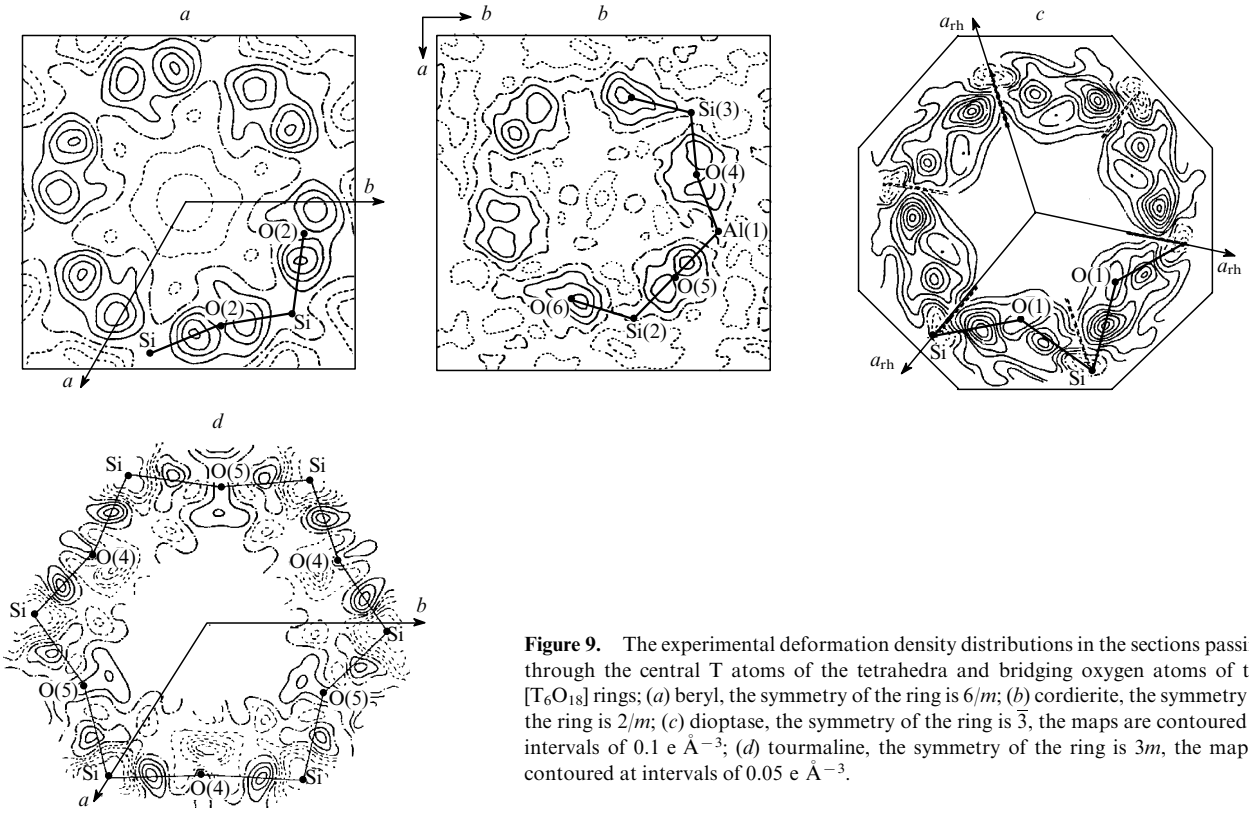


Figure 9. The experimental deformation density distributions in the sections passing through the central T atoms of the tetrahedra and bridging oxygen atoms of the $[T_6O_{18}]$ rings; (*a*) beryl, the symmetry of the ring is $6/m$; (*b*) cordierite, the symmetry of the ring is $2/m$; (*c*) dioptase, the symmetry of the ring is $\bar{3}$, the maps are contoured at intervals of 0.1 e Å^{-3}; (*d*) tourmaline, the symmetry of the ring is $3m$, the map is contoured at intervals of 0.05 e Å^{-3}.

Table 2). At high temperature, these atoms are disordered, which leads to a phase transition. The interatomic Si–O distances in the tetrahedra of these minerals consisting of linked tetrahedra are shorter than those in orthosilicates. According to the rules of electrostatics, the distance between two silicon atoms interacting *via* the bridging oxygen atom is increased due to their repulsion. However, both in beryl and cordierite, all oxygen atoms act as bridges, minerals have the framework structures, the tetrahedral positions are occupied by Be, Si and Al atoms and the above-described effect is not manifested.

For both structures, the deformation electron density maps (see Fig. 9 *a,b*) reveal accumulation of the density at the bridging oxygen atoms. The maxima in the Si–O and Al–O bonds are 0.30–0.40 e Å^{-3} and 0.20–0.25 e Å^{-3}, respectively, which correspond to different electronic structures of the atoms. However, this difference in the Si, Al ring in cordierite is smoothed. Calculations of the error maps demonstrated that these errors were 0.02–0.05 e Å^{-3} in the chemical-bond region and 0.05 and 0.04 e Å^{-3} at the silicon and aluminium atoms, respectively. As in the case of beryl, no difference between the bridging and terminal

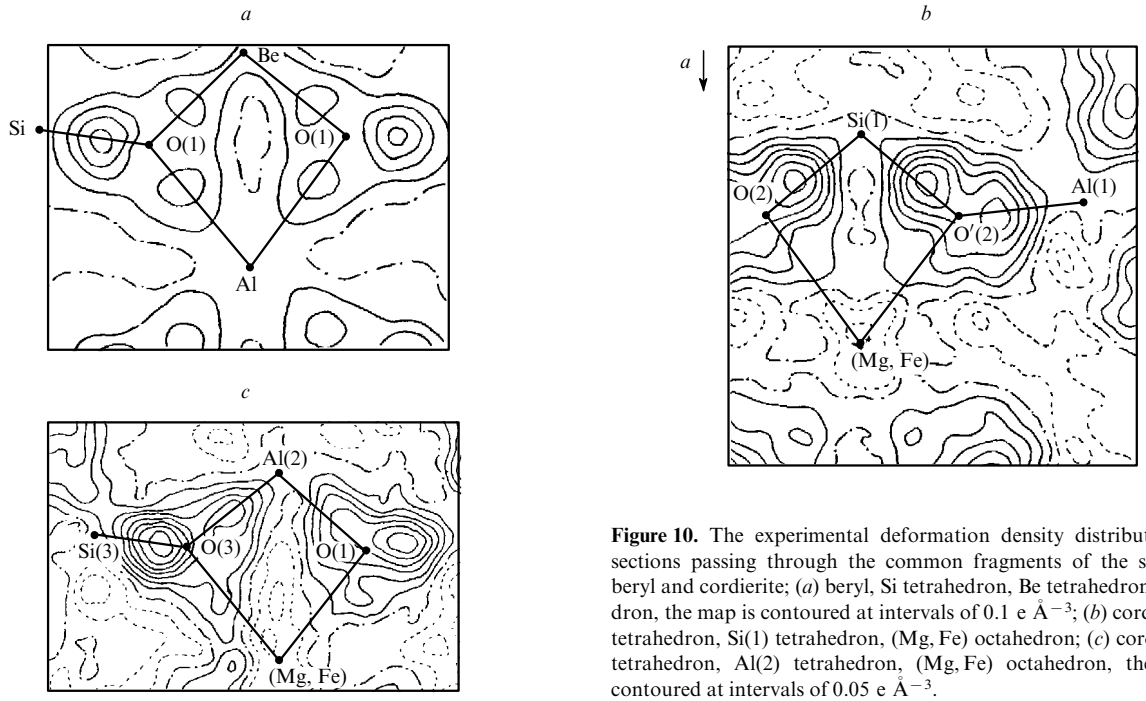


Figure 10. The experimental deformation density distributions in the sections passing through the common fragments of the structures of beryl and cordierite; (*a*) beryl, Si tetrahedron, Be tetrahedron, Al octahedron, the map is contoured at intervals of 0.1 e Å^{-3}; (*b*) cordierite, Al(1) tetrahedron, Si(1) tetrahedron, (Mg, Fe) octahedron; (*c*) cordierite, Si(3) tetrahedron, Al(2) tetrahedron, (Mg, Fe) octahedron, the maps are contoured at intervals of 0.05 e Å^{-3}.

oxygen atoms was observed as regards the values of the maxima in the σ-bonds.

In the framework structure, virtually all oxygen atoms are shared by two tetrahedra. Therefore, the assignment of beryl and cordierite to framework beryllosilicates [55] and framework aluminosilicates, respectively, is valid from the viewpoint of the electronic structure and chemical bonds in these compounds.

The structural fragment common to beryl and cordierite consists of the octahedron (Al or Mg, Fe) and the tetrahedra (Be, Al and Si tetrahedra) linked to the octahedron *via* shared edges or vertices. The differences in the electron density redistribution which occur if the centres of the corresponding polyhedra are occupied by atoms with different electronic structures and electronegativities (Be, Al or Si) [8, 56] are in complete agreement with those expected (Fig. 10): 0.2, 0.2–0.25 and 0.3–0.4 e Å^{-3} for the Be–O, Al–O and Si–O distances, respectively. An increase in the shift of the $\delta\rho$ maxima toward the more electronegative oxygen atom with increasing difference in the electronegativities of the Si–O, Al–O and Be–O pairs of elements allows one to estimate the bond ionicity. In agreement with the traditional crystal-chemical criteria, an increase in the bond ionicity is also observed for the M–O bond in the octahedron where Al is replaced by (Mg, Fe) (see Fig. 10). Note that even a small impurity of iron atoms in the case of hexagonal distortion of the octahedron is manifested in the map as an additional maximum directed toward the threefold axis of the coordination polyhedron, which corresponds to 3*d*-electrons of the iron atom located on the d_{z^2}-orbital (a_g level).

3. Dioptase

The mineral dioptase has the formula $Cu_6[Si_6O_{18}]\cdot 6H_2O$. A specimen of natural dioptase from Kazakstan was studied by the same methods as described above for the specimens of beryl and cordierite.[57] The reflections within a hemisphere of the reciprocal space were reindexed from the hexagonal to the trigonal setting. The rings in silicates under consideration have different symmetry, *viz*., 6/*m*, 2/*m*, $\overline{3}$ and 3*m* in beryl, cordierite, dioptase and tourmaline (discussed below), respectively.

By virtue of the absence of the horizontal mirror plane and corrugation of the $[Si_6O_{18}]$ ring in the case of the symmetry $\overline{3}$, the electron density map for this ring was constructed from fragments (see Fig. 9 *c*). The difference in the Si–O bond lengths in dioptase is consistent with the classical concepts.[8] As in the case of cordierite, the deformation density is accumulated at the bridging oxygen atoms. Of particular interest is the difference in the maxima in the bonds with the participation of the bridging and terminal oxygen atoms (see Fig. 9 *c*,*d*): 0.6–0.8 and 0.2–0.3 e Å^{-3}, respectively (the error in the chemical-bond region is 0.1 e Å^{-3}). These data are indicative of the nonequivalence of the bonds in the silicon–oxygen tetrahedron in dioptase (unlike beryl and cordierite) and underline the role of the bridging oxygen atoms that fasten the corrugated ring as the structural unit in the overall three-dimensional construction. Hence, the characteristic features of the chemical bonds in this mineral confirm the assignment of dioptase to ring silicates.

The structure of dioptase (Fig. 11) is characterised by the presence of corrugated six-membered rings of silicon–oxygen tetrahedra that alternate with analogous six-membered rings of water molecules, which can be considered as the fragments of the ice structure. The positions of the protons in dioptase were determined by neutron diffraction analysis.[58] The electron density distribution in the section passing through the water molecules (Fig. 12 *a*) is similar to the calculated distribution (Fig. 12 *b*) [59] and other experimental distributions. The observed decrease in the electron density on the lone electron pairs is associated with interactions of water molecules with other atoms (in particular, with copper atoms).[60] The calculated geometrical characteristics (bonds and angles) of the hydrogen bonds correspond to the standard values. The hydrogen bonds are directed toward the water molecules within the ring as well as upward and downward

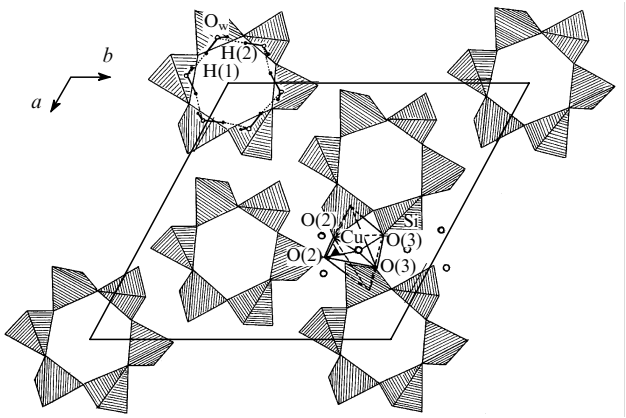


Figure 11. Structure of dioptase.[57]

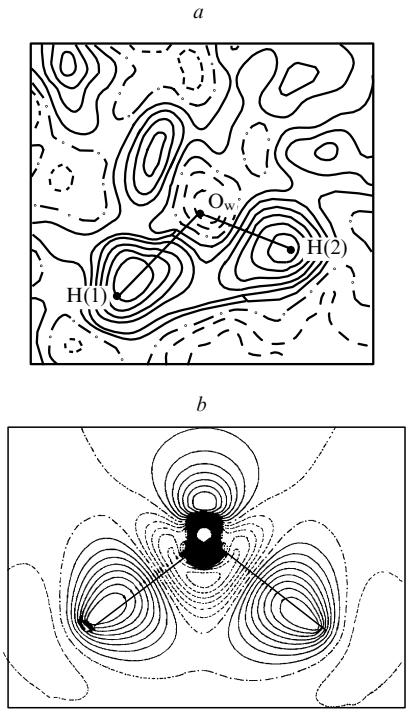


Figure 12. The deformation electron density distributions in the sections passing through water molecules; (*a*) the H(1)–O$_w$–H(2) section (experiment) in dioptase; (*b*) the H–O–H section (calculation) for the isolated water molecule.[59]

(toward the silicon–oxygen rings) thus holding the ring of water molecules in the structure. The experimental and calculated electron densities for the hydrogen bond between two water molecules in the ring are in satisfactory agreement.[61] In the structure of dioptase, unlike the structure of ice (Pauling's model), all lone electron pairs are oriented outward the ring.

In the structure of dioptase, all divalent copper atoms occupy Jahn–Teller-distorted octahedra. The effect of the ligand crystal field on the distribution of the 3*d*-electrons of the copper atom ($[d^9]$ configuration) can be described assuming the symmetry D_{4h} (the true symmetry C_1) of a distorted octahedron. The 3*d*-level splits into 4 sublevels, *viz*., $e_g(d_{xz},d_{yz})$, $b_{2g}(d_{xy})$, $b_{1g}(d_{x^2-y^2})$ and $a_{1g}(d_{z^2})$.[62] When the axes of coordinates are directed along the Cu–ligand bonds with the *z* axis directed toward the apical water molecules, depletion of the $b_{1g}(d_{x^2-y^2})$ orbitals in electron density is observed, all other orbitals being occupied. Hence, in accordance with the Jahn–Teller removal of degeneration, the $a_{1g}(d_{x^2})$ level is stabilised, while the $b_{1g}(d_{x^2-y^2})$ level is destabilised. In

chalcanthite,[63] in which the Cu octahedron possesses a symmetry centre, this pattern is more pronounced.

4. Tourmaline (elbaite)

A specimen of natural tourmaline from Afghanistan was studied by Belokoneva and Tsirelson[64] (see Table 1). Intensities of reflections were measured within a hemisphere of the reciprocal space in the hexagonal setting and, as in the case of dioptase, the reflections were reindexed to the trigonal setting.

The tourmaline family is characterised by a broad spectrum of isomorphism. Five major modifications are distinguished according to the composition and colour of the minerals, *viz*., dravite, elbaite, buergerite, schorl and ulvite.[23] Based on the results of investigations on isomorphism in this specimen and on the results of X-ray microspectral analysis, the formula of tourmaline (elbaite) was established to be $(Na_{0.85}Ca_{0.05})\cdot(Al_{1.10}Li_{1.15}Fe_{0.41}Mn_{0.22}Mg_{0.12})\cdot Al_6B_3Si_6O_{27}(OH)_{3.92}$. The structure of the mineral is shown in Fig. 13.

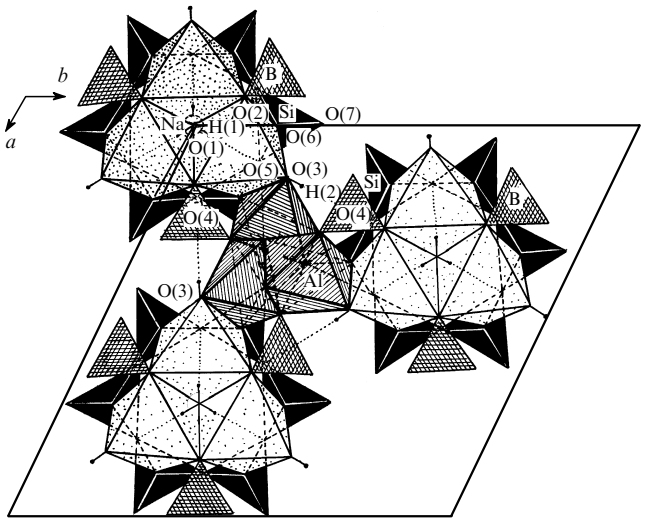


Figure 13. Structure of tourmaline.[64] Dotted hatching indicates (Al, Li, Fe, Mn, Mg) octahedra.

Unlike all the above-considered ring anionic groups which posses a symmetry centre, the ring of silicon – oxygen tetrahedra in tourmaline is polar and corresponds to the symmetry 3*m*. Tourmaline is a pyroelectric mineral.‡ The structural prerequisites for this phenomenon still remain unclear. Hence, analysis of the electron density distribution in the crystal of tourmaline is a topical problem.

The triangular O(4) – O(5) – O(7) faces in the ring of the silicon – oxygen tetrahedra of tourmaline are nearly parallel to the *a* and *b* axes of the unit cell and the polar vertices of the O(6) tetrahedra are located directly above the silicon atoms exactly along the *c* axis. In the silicon-oxygen ring (unlike the analogous rings in the three above-considered minerals), weak $\delta\rho$ maxima are observed in the vicinity of the bridging oxygen atoms (see Fig. 9 *d*), *viz*., outside the ring close to the O(4) atom and within the ring close to the O(5) atom. These maxima correspond to O(H)···O hydrogen bonds. The most remarkable characteristic feature of the deformation density maps is the displacement of the electrons toward the base of the silicon-oxygen tetrahedron with the maximum located directly below the silicon atom (Fig. 14 *a*). In this case, the apical oxygen atom is depleted in electrons in the bond and the $\delta\rho$ maximum is displaced from the bond line

‡ It was in crystals of tourmaline that the phenomenon of pyroelectricity was discovered.

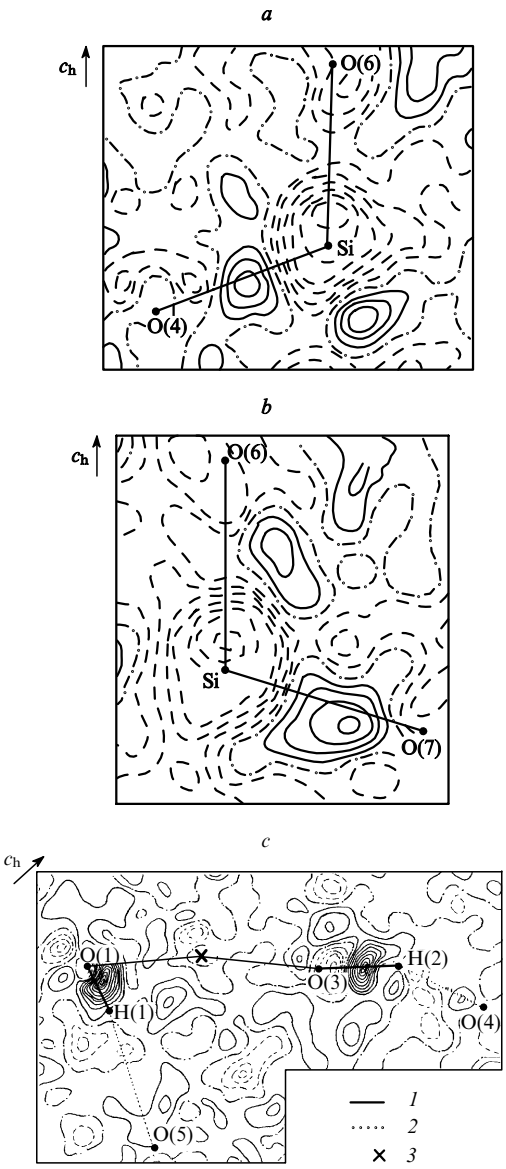


Figure 14. The experimental deformation density distributions in the sections of tourmaline; (*a*) the O(6) – Si – O(4) section with the maximum under the Si atom; (*b*) the O(6) – Si – O(7) section, the maps are contoured at intervals of 0.05 e Å^{-3}; (*c*) O(3) – H(2)···O(4) and O(1) – H(1)···O(5) hydrogen bonds, the map is contoured at intervals of 0.1 e Å^{-3}; (*1*) hydrogen donor, (*2*) hydrogen acceptor; (*3*) the position of the (Al, Li, Fe, Mn, Mg) octahedron.

(Fig. 14 *a*,*b*). The interatomic distance to the apical oxygen atom is shortened, while the distances to the bridging oxygen atoms are elongated (see Table 2). The experimental errors of the determination of the $\delta\rho$ maps in the bond region were 0.06 e Å^{-3}. An asymmetrical charge distribution within the tetrahedron and within the ring as a whole may be responsible for the appearance of an electric dipole moment in the structure and the pyroelectric properties.

The maximum of the deformation electron density was experimentally detected in the $[VOCl_3]$ tetrahedron on the opposite side of the metal – ligand bond,[65] as is the case in the silicon – oxygen tetrahedron in tourmaline. The phenomenon of deformation of the inner electronic shell of the vanadium atom under the action of the polarisation ligand field to produce the local concentration of the charge exterior to the bond was predicted by Bader and co-workers[66, 67] on the basis of the results of quantum-chemical calculations. Apparently, the polarisation field of the oxygen ligands in the ring of tourmaline is responsible

for the unusual deformation electron density distribution and pyroelectric properties.

Tourmaline is a borosilicate the boron atoms of which have a triangular coordination. The electron density distribution in the section passing through the $[BO_3]$ triangle is indicative of the bonds described by the sp^2-hybrid state of the orbitals of the boron atom, which overlap (to form σ-bonds) with the *p*-orbitals of the oxygen atoms.

In the structure of tourmaline, the hydrogen bonds directed from one of the so-called antigorite fragment to another were studied.[3] Figure 14 *c* shows maxima (~ 1 e Å^{-3}) corresponding to the electron density of the hydrogen atoms involved in the O – H bonds. The hydrogen bonds are directed from the O(3) and O(1) donor atoms to the O(4) and O(5) acceptor atoms of the silicon – oxygen ring.

Note that studies of the above-described ring silicates were preceded by only one publication devoted to the investigation of the synthetic analogue of wadeite, $K_2Si[Si_3O_9]$, which contains three-membered rings of Si tetrahedra and silicon atoms in octahedra.[68]

IV. Chain and band silicates

The group of chain and band silicates includes three orthopyroxenes containing a two-membered $[Si_2O_6]$ chain (enstatite, ferroselite and its cobalt analogue),[69] three clinopyroxenes (diopside, $Mg_2Si_2O_6$ and α-spodumene $LiAlSi_2O_6$)[29] and pectolite containing a three-membered chain.[70]

Andalusite, which has been considered by Tsirelson *et al.*[10] in the section devoted to orthosilicates, should be assigned to band aluminosilicates.[71]

The electron density distributions in structures of chain and band silicates have been investigated.[9, 10] Since these publications, this group of silicates has not been supplemented with new members.

V. Sheet silicates

In sheet silicates, bonds between the layers (sheets) are weakened owing to which virtually all these minerals exhibit perfect cleavage. Sheet silicates very rarely occur as faceted crystals. If these crystals do occur, they are strongly flattened along the [0001] direction. When ground to spheres, these crystals either collapse into plates or the spheres obtained give a large diffuse scattering component. For these samples, it is difficult to take proper account of absorption as well as to apply other corrections, which does not allow one to achieve a required precision of experimental data.

A specimen of natural datolite from the Tetuyche deposit (Far East) was studied.[72] The mineral has the layered structure. The configuration of the layer is analogous to that in apophyllite $KCa_4[(Si_4O_{10})_2]\cdot 8H_2O$. Attempts to prepare a spherical sample of the latter mineral, which could give sharp reflections, have failed. In contrast, high-quality spherical samples of datolite crystals were prepared and precision investigation was performed. Intensities of reflections were measured within a hemisphere of the reciprocal space and within an additional hemisphere with $2\theta_{max} = 50°$. The preliminary data processing was carried out with the use of the profile analysis procedure on the basis of Lehmann – Larsen's algorithm. This procedure allows one to obtain more reliable estimations of integrated intensities, particularly, those of weak reflections. Calculations were carried out using the CSD programme.

Microisomorphous relations were studied in the specimen and microimpurities of sodium and iron were detected. The content of the latter correlated with the hydrogen content. The formula of datolite was established to be $(Ca_{0.986}Na_{0.014})Fe_{0.012}\cdot H_{0.988}[BSiO_5]$; its structure is shown in Fig. 15. The incorporation of the iron atoms into the datolite structure indicates that it is related to minerals such as gadolinite and homilite.[23]

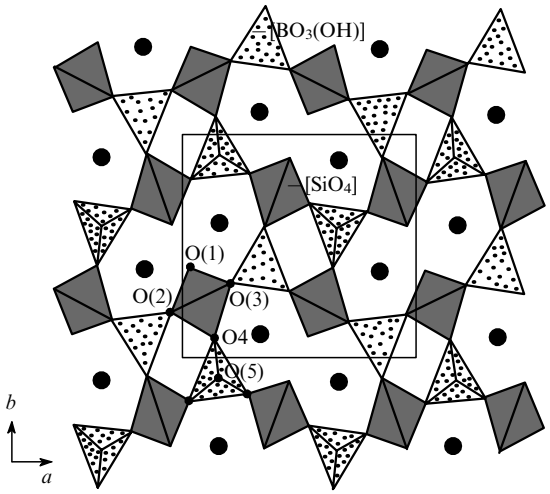


Figure 15. Structure of datolite.[72]

The structure of datolite is built up of silicon – boron – oxygen $[BSiO_5]_\infty$ layers, which consist of tetrahedra linked *via* shared vertices. A characteristic feature of these layers is that the apical vertices of the B tetrahedra occupied by the OH groups are oriented upward and downward with respect to the layer, while the silicon – oxygen tetrahedra are oriented so that their edges are parallel to the layer surface.

Hydrogen bonds were examined on the basis of the electron density maps (Fig. 16) and characterised as bifurcated bonds exhibiting the typical geometrical characteristics. Their crystal-chemical function is to link free vertices of the B tetrahedra and the oxygen atoms in the layer, thus strengthening the boron – oxygen layer.

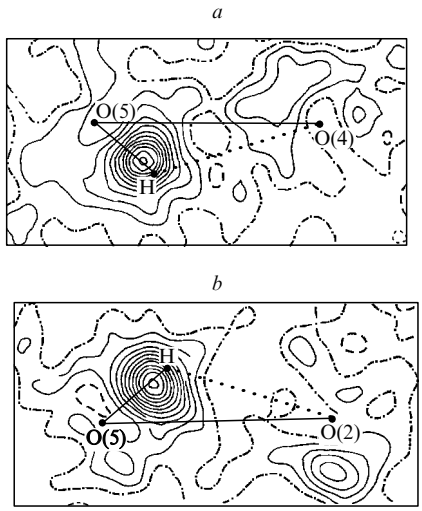


Figure 16. The experimental deformation density distributions in the sections of datolite passing through bifurcated O(5) – H · · · O(4) (*a*) and O(5) – H · · · O(2) (*b*) hydrogen bonds, the maps are contoured at intervals of 0.1 e Å^{-3}.

The deformation electron density distribution in the silicon-oxygen tetrahedron corresponds to the above-described quantum-chemical concepts. The values of the maxima in the bonds vary from 0.25 to 0.40 e Å^{-3} (the average value is 0.35 e Å^{-3}). The $\delta\rho$ distribution is characterised by the presence of electron-density bridges (0.2 e Å^{-3}) between the maxima corresponding to the Si – O bonds [the bridges are parallel to the edges of the tetrahedra and to the layer (Fig. 17 *a*)] and by the absence of such bridges at

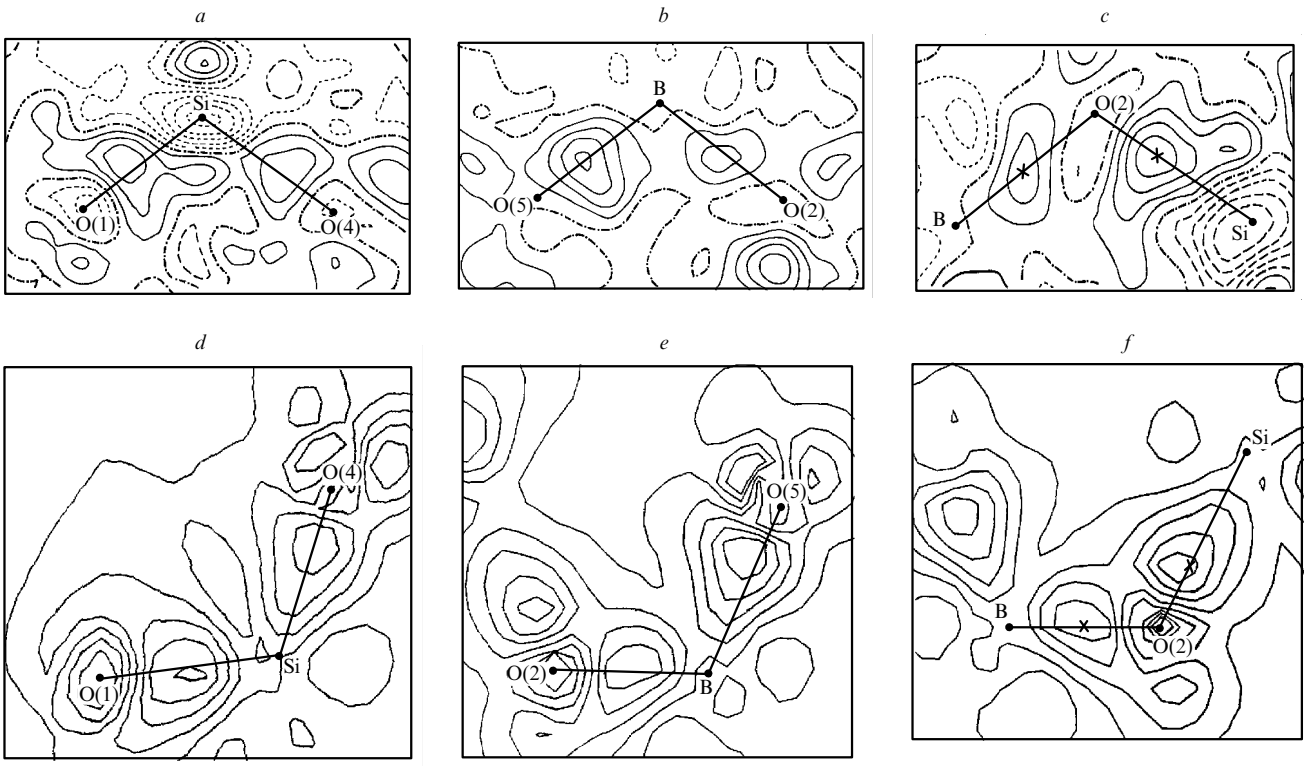


Figure 17. The experimental high-angle (*a*–*c*) and multipole (*d*–*f*) deformation density distributions in the O(1)–Si–O(4) (*a*, *d*), O(2)–B–O(5) (*b*, *e*) and B–O(2)–Si (*c*, *f*) sections of datolite, the maps are contoured at intervals of 0.1 e Å^{-3}. The central points of the peaks are marked with asterisks.

the inclined edges. The electron density distribution in the B tetrahedron (Fig. 17*b*) is similar to that in the silicon–oxygen tetrahedron. The peak heights corresponding to the B–O bonds (on the average, 0.29 e Å^{-3}) are smaller than those corresponding to the Si–O bonds. The difference in the electronegativities of the B–O and Si–O pairs is readily followed from the shifts of the $\delta\rho$ maxima, which are located approximately at the midpoints of the R(B–O) distances and displaced by ~ 0.38 R(Si–O) toward the oxygen atoms (Fig. 17*c*).

The multipole refinement of the datolite structure was performed based on the experimental data reported previously [72] with the use of the MOLDOS96 and SALDOS97 programmes.[44] The refinement characteristics remained virtually unchanged. The calcium atoms were described by monopoles with the wave functions for the Ca^{2+} ion. The calculated static deformation electron density maps agree well with those based on the high-angle model and confirm the principal characteristic features of the electron density distribution in the mineral as well as the crystal-chemical conclusions drawn previously. Thus the static electron density maps for the silicon–oxygen and B tetrahedra have maxima (0.5 e Å^{-3}) corresponding to σ-bonds (Fig. 17*d*,*e*). For the silicon–oxygen tetrahedron, the electron-density bridge (0.1 e Å^{-3}) is clearly seen. The distances from the oxygen atoms to the peaks in the bonds between the bridging oxygen atoms and the silicon and boron atoms are different, *viz*., 0.38 R(Si–O) and 0.50 R(B–O) (Fig. 17*f*), respectively. The bond ionicity can be estimated from the displacement of the peak from the midpoint toward the oxygen atom

$$1-i = 100\frac{r_j/R}{1/2},$$

where i is the ionicity, r_j is the distance from the maximum to the oxygen atom and R is the interatomic distance. For the Si tetrahedron in datolite, the ionicity and covalence calculated by this formula are 24% and 76%, respectively. Note that the static electron density maps match better the theoretical maps than those calculated based on the high-angle model.

The charge on the silicon atom $q = +0.75$ e, estimated in the determination of the population coefficients of valence shells, was lower than that estimated with the use of alternative modern multipole refinement procedures for the structures of silicates.[43] This fact is attributable to the involvement of the *d*-orbitals of the silicon atom in bonding and the presence of the π-component as was suggested by Cruickshank.[11] As a result, the electrons of the *d*-orbital decrease the charge on the silicon atom thus increasing its radius.

As demonstrated above (see Fig. 9*c*), the 'force' (tightening) function of the bridging oxygen atom is manifested in the corrugated silicon–oxygen ring in dioptase. Similarly, chemical bonds in the layer in datolite are also strengthened to retain the layer as a structural unit. In the structure of datolite, layers are linked to each other only *via* bulky polyhedra (Thomson's cubes) about calcium atoms.

For layered silicates, such as kaolinite [74] and lizardite,[75–77] a series of quantum-chemical calculations was performed with the use of the CRYSTAL programme.[78] For kaolinite, the deformation electron density maps were calculated and the characteristics of the oxygen atoms that differ in their crystal-chemical function in the layer were obtained. It was concluded that contributions of the 2*s*- and 2*p*-orbitals of the oxygen atoms to the valence state density dominate over those of the 3*s*- and 3*p*-orbitals of the silicon atoms. The results of calculations of the electron density in the tetrahedral layer of lizardite [75] allowed conclusions to be drawn that both the 3*d*-orbitals of the silicon atoms and the *d*-orbitals of the oxygen atoms play a significant role in bonding. The population coefficient of the *d*-orbital of the silicon atom with the charge of 0.6 e was determined. The charges on the silicon and oxygen atoms calculated with account of the *d*-orbitals agree more closely with the most probable values than those calculated without considering these orbitals.

VI. Framework silicates

1. Coesite

The minerals α- and β-quartz [79,80] and a high-pressure modification of SiO_2, *viz*., coesite,[81,82] belonging to framework silicates were studied by precision methods. The structure of coesite is shown in Fig. 18. In the classical crystal chemistry of silicates, considerable attention is given to the analysis of the Si–O bonds and the Si–O–Si bond angles. Histograms of angles for different structural types were reported, the typical value of the Si–O–Si bond angle was determined (140°; the experimental values are in the range of 120–180°) and the correlations between the bond angles and thermal parameters of the bridging oxygen atoms were treated in the monograph.[8] Coesite is an advantageous subject for precision investigations because it contains crystal-chemically nonequivalent Si–O–Si groups with different geometry (*viz*., the geometry varies from linear with the angle of 180° to bent with angles of up to 137°).[81] The chemical bonds in these groups were studied with the use of the multipole refinement based on Stewart's model. The following deformation electron density distributions were obtained: static (thermal vibrations of atoms were ignored) and dynamic (thermal vibrations were taken into account). For the Si–O–Si groups characterised by the smallest angles (142° and 137°), the electron density bridges between the maxima in the bonds were observed; these bridges were located within the bent Si–O–Si fragment (Fig. 19 *a*,*b*).

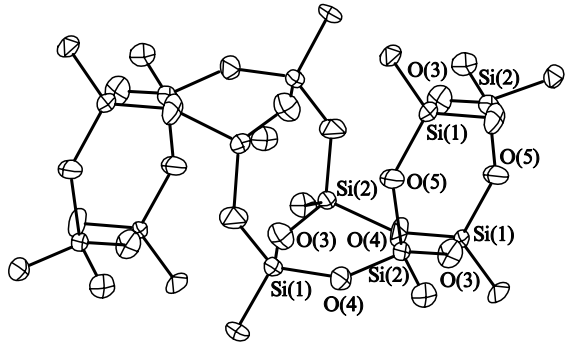


Figure 18. Structure of coesite.[81]

A diversity of crystal-chemically different Si–O–Si groups in the structure of coesite made it possible to reveal the regularities relating the bond lengths to the bond angles in these groups. The results of precision investigations demonstrated that the linear group is characterised by the shortest Si–O distances, the electron density symmetrically 'enveloping' the bridging oxygen atoms. The Si–O bond length increases and a bond bridge appears within the angle as this angle decreases. The transfer of the electron density and formation of a bond bridge within the Si–O–Si angle are manifested in the electron density distribution map of dioptase (see Fig. 9 *c*). In dioptase, the Si–O–Si angle in the ring (132.77°) is smaller and the average bridging Si–O distance (1.609 Å) is larger than the corresponding values in beryl (167.99° and 1.633 Å, respectively; see Table 2). In beryl, the electron density almost uniformly envelopes the bridging oxygen atom (see Fig. 9 *a*).

In the dependence of R(Si–O) on $1/[1-\sec(\text{Si–O–Si})]$, all points determined in calculations [8,11] for different angles lie along a straight line which runs parallel and below the experimental straight lines constructed on the basis of the results of multipole refinement. This fact is indicative of the possible participation of the 3*d*-orbitals of the silicon atom in bonding. A comparison of the dynamic and static experimental and calculated $\delta\rho$ maps demonstrated that they are basically alike.

The structure of coesite was reinvestigated by Downs in more detail.[82] This investigation was also performed with the use of Stewart's model (VALRAY programme) but another monopole was specified and a different number of parameters were finally refined. Maps of the experimental full electron density and of the total and deformation electrostatic potentials were calculated in addition to static maps $\delta\rho$. The radii of best separation (bonded radii) were estimated from the full electron density distributions analogously to that described in Refs 38, 45. The silicon and oxygen radii were found to be 0.68 and 0.94 Å, respectively. These values are close to those determined previously and differ from Shannon–Prewitt's radii [83] estimated for an ionic model. Analysis of the $\delta\rho$ distributions in the static maps for different Si–O–Si angles revealed (as in Ref. 81) that the density accumulated as bridges at the Si–O(2) and Si–O(5) bonds (the smaller Si–O–Si angles) and its transfer inward the angle. For the O(5) atom, which is characterised by the minimum bond angle, the maximum is also observed in the nonbonding region (Fig. 19 *c*). The perpendicular section was not reported by Downs.[82] However, it was suggested that the O(5) atom is sp^2-hybridised, which invokes an additional reasoning.

The electrostatic potential maps in the vicinity of different bridging oxygen atoms are not the same. This confirms the general conclusion that long-range interactions should be taken into account in calculations of catalytic properties. These interactions affect substantially the local density and, consequently, the probability of localisation of an impurity. Using coesite as an example, let us note that dynamic models which include the monopole term of the multipole function as a subtrahend [81] are close to models used in high-angle refinement. From the viewpoint

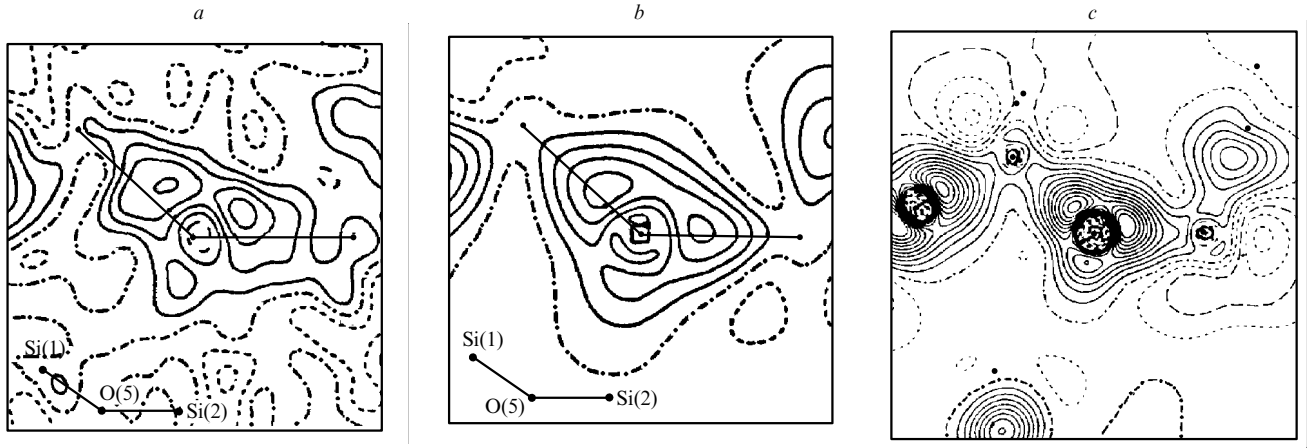


Figure 19. The experimental deformation density distributions in the Si(1)–O(5)–Si(2) section of coesite; (*a*) dynamic density; (*b*) static density,[81] (*c*) static density (multipole refinement);[82] the maps are contoured at intervals of 0.1 e $Å^{-3}$.

of characteristic features of chemical bonds, dynamic models are as informative as static multipole models.

2. Danburite

A natural specimen of danburite from Japan was studied.[84] The structure of danburite $CaB_2Si_2O_8$ is shown in Fig. 20. The investigation of the tetrahedral borosilicate framework was of prime interest. The calcium atoms were described by a monopole with the wave functions for the Ca^{2+} ion. The complete and difference electron density distributions as well as their topological characteristics and the electrostatic potential were calculated and examined. Unfortunately, the complete three-dimensional and, particularly, difference maps contained numerous small split peaks and hence, their quality was poorer compared to those reported, for example, by Geisinger *et al.*[81] Downs and Swope[84] noted this fact and gave preference to the multipole model because it can serve as a 'filter' for experimental results of poor quality. The main aim of the cited work was to determine the topological characteristics. For borosilicate, these characteristics were determined for the first time. However, the conclusion, which was drawn on the basis of these data according to Bader's theory, that the ionic component prevails in the bonds (closed shell interactions) in danburite (as in topaz) is inconsistent on the whole with the commonly accepted view of the predominantly covalent character of these bonds. Possibly, new investigations as well as a deeper insight into the essence and interpretation of the topology of chemical bonds in complex structures of silicates will help in explaining this disagreement.

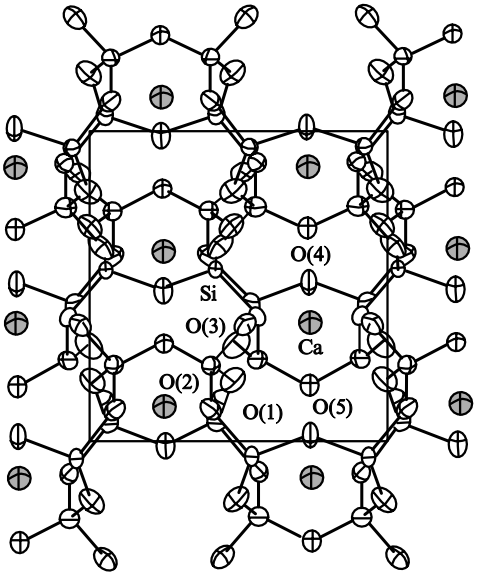


Figure 20. Structure of danburite.[84]

3. Natrolite

Natrolite $Na_2Al_2Si_3O_{10} \cdot 2H_2O$ is a framework silicate belonging to zeolites. Specimens from the Czech Republic were studied.[85–87] The mineral was originally investigated with the use of the high-angle refinement[85,86] (see §) and then studied with the use of the multipole analysis procedure.[87] Zeolites are characterised by a high degree of disorder, which precludes precision investigations of these minerals. However, natrolite is characterised by the ordered distribution of the silicon and aluminium atoms in the framework as well as of the sodium atoms and water molecules within the channels. The deformation electron density distributions were calculated with the use of the CRYLSQ, FOURR and SADIAN90 programme packages. Stuckenschmidt and co-workers[86] tested different modes of refinement and gave preference to atomic scattering curves for half-ionised atoms. All necessary corrections were applied and errors of the electron density maps were evaluated. Natrolite was described[86] as an aluminosilicate studied for the first time without considering the results of investigations reported previously.[47,51] However, the characteristic features of the chemical bonds under consideration as well as the conclusions made agree well with the results of other studies.[47,51] On the basis of the shift of the $\delta\rho$ maximum, it was established that the Al–O bond is more ionic than the Si–O bond in accordance with the electronic structures of the Al and Si atoms, and the height of this maximum is smaller (Fig. 21 *a*,*b*). The distances to the maxima in the bonds (M) in the tetrahedra are identified with the radii of the overlapping orbitals in the silicon–oxygen tetrahedra ($\langle SiM \rangle$ = 0.90 Å and $\langle OM \rangle$ = 0.73 Å) and Al tetrahedra ($\langle AlM \rangle$ = 1.09 Å and $\langle OM \rangle$ = 0.70 Å). The radii of

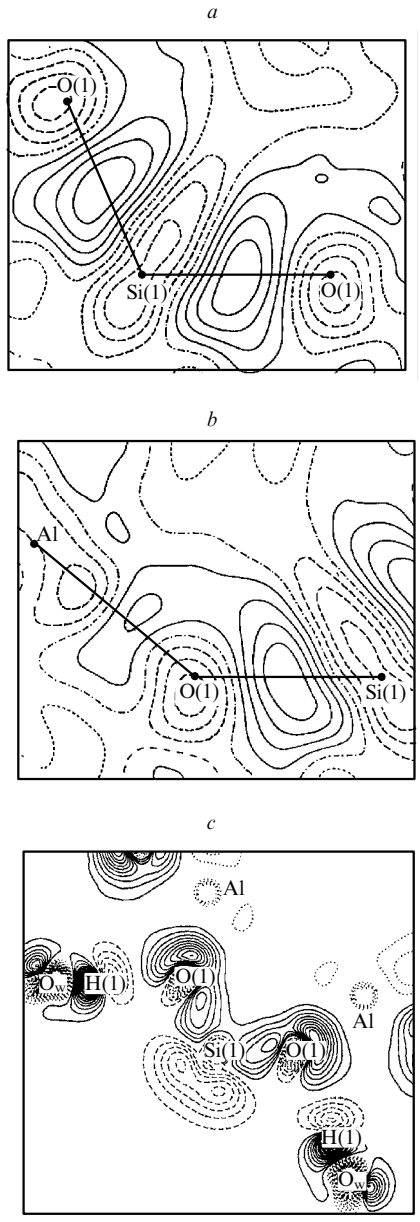


Figure 21. The experimental deformation density distributions in the O(1)–Si–O(1) (*a*) and Al–O(1)–Si(1) (*b*) sections (the maps are contoured at intervals of 0.1 e Å^{-3})[86] and the static deformation density distribution in the Si(1)–O(1)–Al section (*c*) (the map is contoured at intervals of 0.05 e Å^{-3})[87] in natrolite.

§ The experiment was detailed in the former study and the deformation density was examined in the latter study.

the silicon and aluminium atoms thus determined agree with the calculated maximum radii of the outer orbitals (0.904 and 1.044 Å for the 3*s*-orbitals of Si and Al, respectively). However, the radii for the 3*p*-orbitals have larger values (1.068 and 1.312 Å for Si and Al, respectively). It can be suggested that the values of the radii of overlapping hybrid orbitals are intermediate between the above values. It was concluded [86] that the maxima in the bonds are located at positions predicted for a covalent bond in tetrahedra.

The interest in studies of the electron density and electrostatic characteristics of zeolites stems from the fact that this group of silicates posseses ion-exchange properties. With the aim of relating the characteristics of natrolite to the ion-exchange properties, the multipole refinement of the structure of natrolite was carried out, the charges on the atoms were estimated and the electrostatic potential was examined.[87] General approaches and refinement procedures were detailed. All necessary corrections were applied to the experimental data (see Table 1). The multipole refinement was carried out using Hansen – Coppens's model and the MOLLY programme. The choice of the system of coordinates on atoms and the number of refinable multipole parameters were described in detail and the coefficients of radial functions were reported. The isotropic extinction, the scale factor, the positional and anisotropic thermal parameters of the atoms, the population coefficients of valence (P_v) and multipole (P_{lm}) orbitals and their contraction-expansion parameters (æ and æ′, respectively) were refined.

In the calculated static multipole maps (STATDENS programme), the deformation density is concentrated at more electronegative oxygen atoms (Fig. 21 *c*). The maxima in the Si – O and Al – O bonds are 0.25 and 0.45 e Å^{-3}, respectively, although an inverse ratio, which is in better agreement with the electronic structures of the silicon and aluminium atoms, had been obtained previously. The shifts of the maxima toward the oxygen atoms correspond to the difference in the electronegativities of the oxygen and silicon atoms and of the oxygen and aluminium atoms and are consistent with a more covalent character of Si – O bond. The electrons of the silicon atoms occupy the sp^3-bonding orbitals. Regions of localisation of the electron density of the hydrogen atoms and the lone electron pairs of the water molecules are clearly seen in the maps (see Fig. 21 *c*). Ghermany and co-workers [87] calculated the charges on the atoms, reported the maps of the total potential and determined the electrostatic energy of the sodium atoms in the structure of natrolite. A comparison of the latter characteristic with an analogous value for dehydrogenated zeolite A demonstrated that the Na^+ ion is more tightly held in the crystal structure of natrolite.

4. Phenakite

The results of studies of the electron density of phenakite Be_2SiO_4 were considered earlier [10] in the section devoted to island silicates. However, investigations of the character of chemical bonds demonstrated [33, 34, 88] that phenakite belongs to framework beryllosilicates (Fig. 22). In the studies [33, 34] published almost simul-

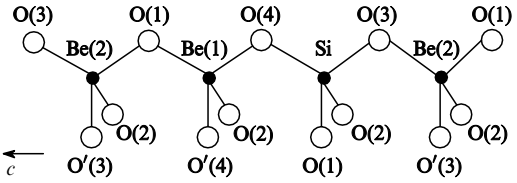


Figure 22. A fragment of the phenakite structure.

taneously, the deformation electron density distributions (Fig. 23 *a*,*b*) were calculated with the use of high-angle and multipole models. The dynamic and static maps were reported.[34] It was demonstrated that the Si – O and Be – O chemical bonds possess different ionicities (in accordance with the classical concepts of the electronegativies of pairs of interacting atoms). The difference in the maxima in the bonds (0.2 and 0.4 for Be – O and Si – O, respectively) and their substantial shifts toward the oxygen atom along the Be – O bond compared to the Si – O bond are clearly seen in the electron density distribution maps for the structure of phenakite (like beryl). The static density maps more closely resemble the calculated maps compared to the dynamic density maps.

The multipole refinement with the use of the æ-technique allowed the determination of charges on atoms in silicates for the first time.[34] The deformation [33] and total electrostatic [34] potentials

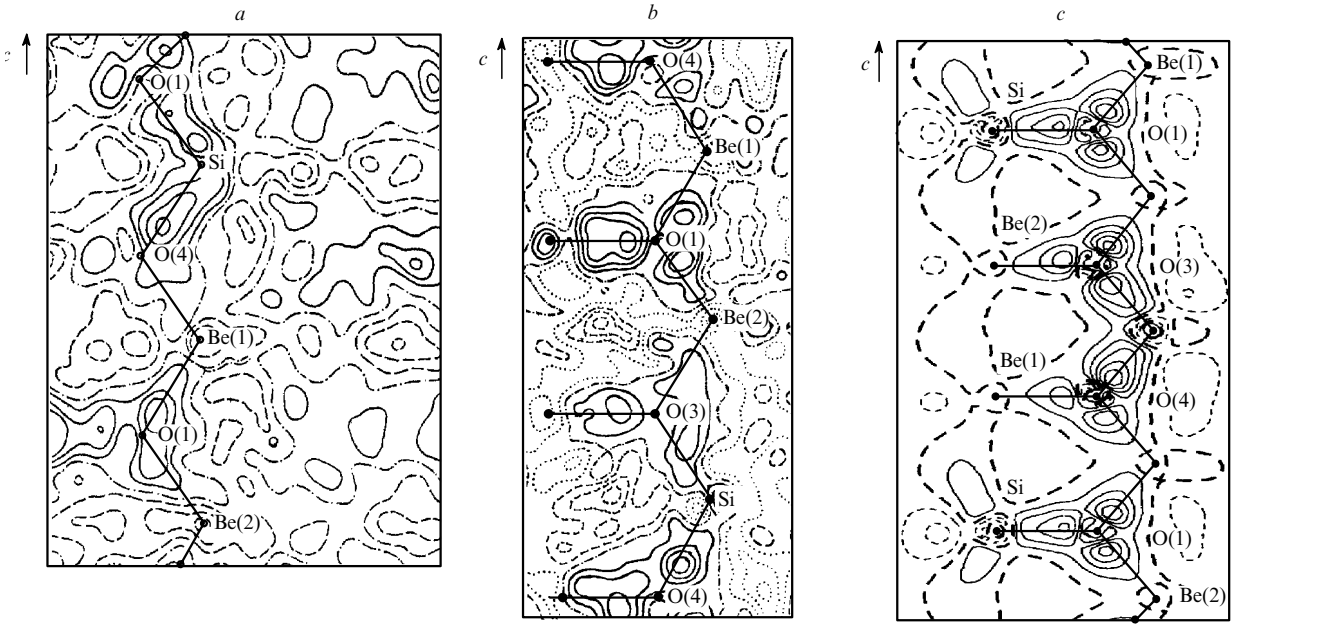


Figure 23. The experimental deformation density distributions in the sections of phenakite passing through ...Si – O(4) – Be(1) – O(1) – Be(2) – O(3) – Si... chains; (*a*) according to Ref. 33; (*b*) according Ref. 34; (*c*) the static multipole refinement based on the experimental results.[33]

were determined, which made it possible to reveal the electrostatic properties of beryllium and silicon.

Recalculations for phenakite were performed with the experimental results [33, 34] using Hansen – Coppens's model with the use of the MOLDOS96 and SALDOS97 programme packages. The potential and topological characteristics of this mineral were also calculated. The static deformation maps (Fig. 23 *c*) as well as the charges on the atoms agree on the whole with the bonding pattern reported previously.[33, 34]

VII. Quantum-chemical calculations of selected framework structures

The structure of neither danburite nor natrolite was calculated by the quantum-chemical methods, while the completely dealuminated form of zeolite $Si_{48}O_{96}$, *viz*., mordenite $(Ca,Na_2,K_2)[AlSi_5O_{12}]_2 \cdot 6H_2O$, was investigated by these methods.[89] The results obtained in independent studies were used as the initial data in *ab initio* calculations (CRYSTAL programme). It was found that the bond strain increases as the bond angle decreases, which agrees with the results of studies of chemical bonding in coesite and dioptase (the appearance of the above-described bridges). According to the results of calculations of the valence state density, the deformation and full density maps were constructed (Fig. 24). The results of determination of the sizes of cavities (chains) along the *c* axis with the use of isosurfaces of the complete density are intriguing. The diameter of the cavities (~ 7 Å) agrees well with the experimental values. Analysis of the characteristics of the potentials with the aim of predicting the behaviour of extraframework species (guests) demonstrated that the cations are preferentially located in the vicinity of the edges of large channels rather than in their centres.

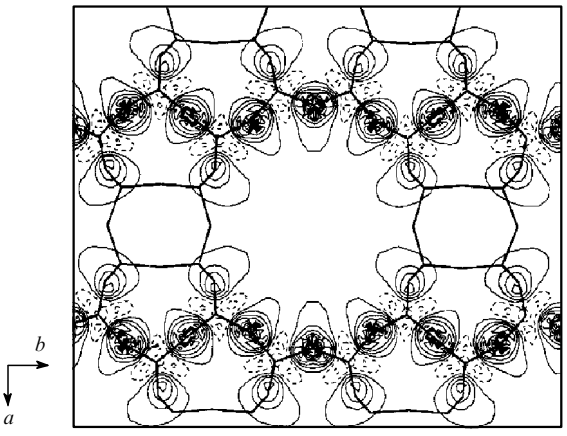


Figure 24. The deformation density distribution in the section of mordenite (calculation).[89]

Quantum-chemical calculations of various frameworks were carried out for the $H_6Si_2O_7$ molecule.[90] Starting from four SiO_2 units, 23 tetrahedral framework structures characterised by different symmetry and different unit-cell dimensions were found from local energy minima. Initially, triclinic symmetry was assumed for these structures. However, only seven structures under study have this symmetry. The symmetry groups of other structures varied from monoclinic (*Pc*) to cubic (*I*43*d*).

Gibbs and co-workers [91] carried out quantum-chemical (Hartree – Fock self-consistent field) calculations of electron densities and the topology of the electron density of the molecules of 'polysilicic acids,' *viz*., $Si^{I}O$, $Si^{II}O_2$, $H_4Si^{IV}O_4$, $H_6Si_2{}^{IV}O_7$, $H_8Si^{VI}O_6$, $H_{10}Si_2{}^{VI}O_{10}$ and $H_{12}Si^{VIII}O_8$ (the coordination number of the silicon atom is designated by a Roman numeral). The effect of the bond length on the values of the maxima in the bonds as well as the bond ionicity and atomic charges were examined. It was found that the bond ionicity increases as the coordination number of the silicon atom increases. On the contrary, the covalent character of the bond and the values of the bond maxima increase as its length decreases and the Si – O – Si angle increases. Thus the $\rho(r)$ value at the critical point in the bond as determined in topological analysis increases from 0.50 e Å^{-3} for the Si – O distance of 1.96 Å in the octahedron to 0.92, 0.95 and 1.36 e Å^{-3} for the Si – O distances of 1.621, 1.595 and 1.48 Å, respectively, in the tetrahedron. The ionic (crystal) radius of the oxygen anion is not a constant and increases from 0.86 Å at R(Si – O) = 1.48 Å to 1.20 Å at R(Si – O) = 1.96 Å. The atomic charge increases in accordance with an increase in the size of the ion because the atomic 'reservoir' and the bond ionicity increase. It was demonstrated that the bond ionicity could be estimated by determining the bonding radius of the anion from electron density maps using the Gibbs empirical formula

$$f_i(XO) = 1.0 - \exp\left\{-\tfrac{1}{4}[-0.85 + 2.64 r_b(O)]^2\right\},$$

where r_b(O) is the bonding radius. It was also concluded that weak π-bonds ($p-d$) are formed due to the involvement of the atomic 3*d*-orbital of the silicon atom the contribution of which increases as the angle decreases and the bond strain increases, as described for coesite, dioptase and datolite.

Worthy of mention are also calculations of the structures of ilmenite $MgSiO_3$ [92, 93] and a high-pressure modification of stishovite.[94, 95] The silicon atoms in these minerals occupy octahedra. Different computational methods were used, which supplemented investigations [96, 97] on the electron density of this unusual modification of SiO_2 (stishovite) analogous to rutile.

VIII. Determination of charges on atoms in silicates

In structural chemistry, the notion of the charge on the atom is closely associated with the notion of the ionic radius and with the development of the concept of the bond ionicity. Liebau [8] recalled that according to Pauling the ionicity of the Si – O bond was evaluated at 50%. In the work of Stewart and co-workers [79] cited in the monograph,[8] the ionicity *i* was defined as the ratio of the residual (effective) charge to the formal charge expressed in percent. Thus if the residual charge on the silicon atom is equal to +1, then $i = 25\%$. Consequently, four very similar bonds are each 75% covalent.[79] The charges on the silicon and oxygen atoms can be independently determined from the data of direct precision X-ray diffraction studies or from the results of quantum-chemical calculations. The CRYSTAL programme package opens up possibilities of calculations for not only clusters but also periodical systems. Model charges on atoms can be also determined according to correlation formulas from the positions of lines in X-ray emission spectra.

For the purpose of evaluating charges in some silicates from precision X-ray diffraction data, Fujino and co-workers [27] proposed a procedure according to which the number of electrons was initially determined for cations within a sphere corresponding to the effective radius based on radial distributions of difference maps. Then, it was proposed to apply a procedure according to which the charge of the cation determined by the above procedure was fixed, the neutrality of the crystal was prescribed and atomic scattering factors of oxygen atoms were refined. In such a manner charges in a series of island and chain silicates were determined. For oxygen atoms, the values vary from −1.1 to −1.5 e and the charge for the silicon atom is +1.4 e. For wadeite, these values were found to be higher (−1.43 and +3.29 e for oxygen and silicon, respectively).[68] The similar values (−1.8 and +3.5 e, respectively) were obtained for dioptase. The electron density was integrated within a sphere about the atom with the radius of the best separation found from valence density maps (with the use of

the MINEXTL programme package); however, the charges varied too sharply as the radii were changed.

The best procedure for the determination of the charges involves the multipole refinement of the population coefficient P_v simultaneously with the parameter æ′, which characterises 'contraction' (æ′ > 1) or 'expansion' (æ′ < 1) of the atom. The values of the charges with the use of the æ-technique and the VALRAY programme were calculated for the first time for phenakite.[34] For oxygen and silicon, these charges are, on the average, −1.01 and +1.49 e, respectively. Calculations for the layer in lizardite using the CRYSTAL programme gave the following charges on the silicon atom: +2.39 e when the *d*-orbitals of the silicon atom were ignored and +1.66 and +1.58 e when these orbitals were taken into account. For the structure of datolite, the values obtained from the experimental results were lower than those for other silicates:

Atom	Si	B	O(1)	O(2)	O(3)	O(4)	O(5)
Charge /e	+0.75	+0.84	−0.71	−0.66	−0.76	−0.72	−0.66

In this case, the charge on the calcium atom was taken to be equal to +2 (by analogy with danburite). In natrolite, the charge on the sodium atom was taken as equal to +1 and the charges on two independent silicon atoms were found to be +1.84 and +1.65 e, the charge on the aluminium atom was +1.51 e and the charges on the O(1), O(2) and O(3) atoms were −0.73, −1.08 and −0.99 e, respectively, for the values of the æ′ parameter corresponding to a slight contraction of the shell of the silicon atom and expansion of the shell of the oxygen atom. Note that after the multipole refinement, the refinement of only P_v and æ′ was repeated, *i.e.*, the total multipole component that corresponds to the density in the bond was excluded. This procedure was not performed for danburite. As a consequence, the P_v values reported involve the multipole component and are unsuitable for the estimation of charges. For natrolite, the determined charges were compared with those calculated for α-quartz. In α-quartz, the charges on the silicon and oxygen atoms vary from +2.4 to +1.6 e and from −1.13 to −0.83 e, respectively. Calculations for topaz performed with the use of a procedure analogous to that used for natrolite gave the following effective charges:

Atom	Al	Si	O(1)	O(2)	O(3)	F
Charge /e	+1.53	+1.75	−0.76	−1.11	−1.03	−0.44

For phenakite, the charges were calculated using two experimental data sets (I and II):[88]

Atom	Si	Be(1)	Be(2)	O(1)	O(2)	O(3)	O(4)
Charge (I) /e	+1.12	+1.19	+1.19	−0.87	−0.88	−0.87	−0.89
Charge (II) /e	+0.87	+1.53	+1.26	−0.90	−0.95	−0.91	−0.89

The charges obtained in the multipole refinement agree most closely with the real charges on atoms. A comparison of these values with each other as well with the results of quantum-chemical calculations demonstrated that the most typical values for the silicon and oxygen atoms are in the ranges of +1.1 to +1.8 e and of −0.7 to −1.1 e, respectively. Thus, in spite of the indefiniteness of the notion of the charge on the atom, it is applicable for semiquantitative estimations in structural chemistry. According to the new data on the charges, the Si−O bond ionicity determined with the use of equations given in Ref. 79 was ∼33% with a correspondingly higher degree of covalence (∼67%). Undoubtedly, this line of investigation is of interest.

IX. Conclusion

The data of precision X-ray diffraction studies allow one to take a new view of problems associated with investigations of structures and bonds in silicates and their classification. From the structural standpoint, positional and thermal parameters can be determined with a better accuracy, isomorphous relations in silicates can be examined with the use of electron density distribution maps by determining structural positions of small amounts (less than 1 mass %) of impurities, in particular, of chromophore ions responsible for the colour of crystals, and hydrogen bonds can be reliably localised to the extent that positions of electrons of hydrogen atoms and lone electron pairs of oxygen atoms in water molecules can be revealed.

The experimental and calculated electron density distribution maps demonstrate that in the case of formation of a chemical bond in the silicon – oxygen tetrahedron as well as in the B, Al and Be tetrahedra, the electrons of these atoms occupy the sp^3-bonding orbitals to form σ-bonds with the oxygen atoms, which corresponds to the classical concepts. In special cases, which require strengthening (strain) of the bond, in particular, in a silicon – oxygen layer, in a corrugated isolated ring of dioptase or in strained bonds with a small Si−O−Si angle in the coesite framework, it was assumed that the 3*d*-orbitals of the silicon atom are involved in bonding with a contribution of the π-component to the bond. The presence of the π-component may account for the existence of electron-density 'bridges' in the silicon – oxygen tetrahedra in dioptase, datolite and coesite (for the last-mentioned mineral, this fact is also confirmed by calculations).

The values of the $\delta\rho$ maxima correlate with the electronic structures of the elements. In most instances, the values of the maxima for the silicon atom vary within a rather narrow range (0.3 – 0.4 e $Å^{-3}$) for various structures examined in different studies, which is indicative of the reliability of the results. The differences in the values may occur due to the characteristic features of the structures of compounds under study and chemical interactions in them.

The deformation density distribution maps for tetrahedra visualise the effect of the difference in the electronegativities of the elements involved in chemical bonding. In the B−O, Si−O, Al−O and Be−O series, an increase in the ionicity for these primarily covalent bonds can be quantitatively estimated. The effective radii of atoms, their effective charges (for the silicon and oxygen atoms, the most probable values are in the ranges from +1.1 to +1.8 e and from −0.7 to −1.1 e, respectively) and the Si−O bond ionicity can be quantitatively estimated from the $\rho(\mathbf{r})$ maps.

The traditional classification of silicates in accordance with the degree of condensation of anionic groups and the regularities of changes in the bond lengths and bond angles[8] correlate with their electronic structures. Thus cations of the second coordination sphere play the major role in orthosilicates. These cations cause a change in the values of the $\delta\rho$ maxima and their shifts up to splitting. On condensation of tetrahedra, the electron density is accumulated at the bridging oxygen atoms. When all oxygen vertices are shared, the maxima in all four bonds are equal. This equality is disturbed in the case of formation of isolated tetrahedral groups, for example, rings.

Investigations of electron density distributions make it possible to consider the fundamentals of the traditional structural chemistry of silicates on the electronic level. Specifically, a particular classification of structures can be chosen taking into account the character of the electron density distribution.

Due to intensive development of computational quantum-chemical procedures in recent years, these procedures approach the accuracy of experimental methods and make it possible to perform a semiquantitative comparison of the results of two methods with the use of density maps and populations of orbitals. These combined investigations can provide most reliable data on structures of complex silicate systems on the electronic level.

Refernces

1. P P Evald (Ed.) *Fifty Years of X-Ray Diffraction* (Utrecht: International Union of Crystallography, 1962)
2. U L Bragg, G F Klaringbull *Crystal Structures of Minerals* (London: Bell and Sons, 1965)
3. N V Belov *Ocherki po Strukturnoi Mineralogii* (Essays on Structural Mineralogy) (Moscow: Nedra, 1976)
4. V T Tsirel'son *Elektronnaya Kristallokhimiya. Kristallokhimiya (Itogi Nauki i Tekhniki)* [Electronic Crystal Chemistry. Crystal Chemistry (Advances Science and Engineering Series)] (Izd. VINITI, Moscow: 1986) Vol. 20
5. V T Tsirel'son *Khimicheskaya Syaz' i Teplovoe Dvizhenie Atomov v Kristallakh. Kristallokhimiya (Itogi nauki i tekhniki*) [Chemical Bond and Thermal Movement of Atoms in Crystals. Crystal Chemistry (Advances Science and Engineering Series)] (Izd. VINITI, Moscow: 1993) Vol. 27
6. V G Tsirelson, R P Ozerov *Electron Density and Bonding in Crystals* (Bristol, Philadelphia: Institute of Physics Publishing, 1996)
7. Ph Coppens *X-Ray Charge Densities and Chemical Bonding (International Union of Crystallography, Text of Crystallography)* (Oxford: Oxford Science Publications, 1997)
8. F Liebau *Structural Chemistry of Silicates, Structure, Bonding and Classification* (Berlin: Springer, 1985)
9. V G Tsirel'son, O A Evdokimova, E L Belokoneva, V S Urusov *Zap. L'vovsk. Miner. O-va. Miner. sb.* **43** (2) 3 (1989)
10. V G Tsirelson, O A Evdokimova, E L Belokoneva, V S Urusov *Phys. Chem. Miner.* **17** 275 (1990)
11. D W J Cruickshank *J. Chem. Soc.* 5486 (1961)
12. M E Dyatkina *Osnovy Teorii Molekulyarnykh Orbitalei* (Foundations of the Theory of Molecular Orbitals) (Moscow: Nauka, 1975)
13. N K Hansen, Ph Coppens *Acta Crystallogr., Sect. A* **34** 909 (1978)
14. R F Stewart, M A Spackman *VALRAY Users Manual* (Pittsburg, PA: Carnegie-Mellon University, 1983)
15. Ph Coppens, W C Hamilton *Acta Crystallogr., Sect. A* **26** 71 (1970)
16. Ph Coppens, T N G Row, P Leung, E D Stevens, P J Becker, H W Yang *Acta Crystallogr., Sect. A* **35** 63 (1979)
17. R Olthof-Hazekamp *CRYLSQ Xtal3.0. Reference Manual* (Eds R S Hall, J M Stewart) (Perth: University of the Western Australia and Maryland, 1990)
18. J M Stewart, J Holden, R Doherty, R S Hall *FOURR Xtal3.0. Reference Manual* (Eds R S Hall, J M Stewart) (Perth: University of the Western Australia and Maryland, 1990)
19. W H Baur, D Kassner *Z. Kristallogr., Suppl. Issue (SANDIAN90 Prepares Input for DLS-76)* 15 (1991)
20. R G Gerr, T N Borovskaya, I V Voloshina, N N Lobanov, O L Slovokhotova, V A Strel'tsov, Yu T Struchkov, R P Ozerov, V P Tsirel'son, A I Yanovskii *Zh. Strukt. Khim.* **32** 170 (1991) [a]
21. T Koritsansky, S Howard, T Richter, Z Su, P R Mallinson, N K Hansen *XD, a Computer Program Package for Multiple Refinement and Analysis of Electron Density from X-Ray Diffraction Data* (Berlin: Free University, 1995)
22. W L Bragg *Z. Kristallogr.* **74** 237 (1930)
23. H Strunz *Mineralogische Tabellen* (Leipzig: Academie Verlag, 1970)
24. A S Povarennykh *Kristallokhimicheskaya Klassifikatsiya Mineral'nykh Tipov* (Crystal Chemical Classification of Mineral Types) (Kiev: Naukova Dumka, 1966)
25. D Yu Pushcharovskii *Strukturnaya Mineralogiya Silikatov i Ikh Sinteticheskikh Analogov* (Structural Mineralogy of Silicates and Their Synthetic Analogs) (Moscow: Nedra, 1986)
26. H Fuess, J W Bats, W Joswig *Z. Kristallogr.* **156** 41 (1981)
27. K Fujino, S Sasaki, Y Takeuchi, R Sadanaga *Acta Crystallogr., Sect. B* **37** 513 (1981)
28. A Kirfel, G Will *Z. Kristallogr.* **159** 73 (1982)
29. S Sasaki, K Fujino, Y Takeuchi, R Sadanaga *Acta Crystallogr., Sect. A* **36** 904 (1980)
30. O Tamada, K Fujino, S Sasaki *Acta Crystallogr., Sect. B* **39** 692 (1983)
31. F Marumo, M Isobe, S Akimoto *Acta Crystallogr., Sect. B* **33** 713 (1977)
32. F Marumo, M Isobe, Y Saito *Acta Crystallogr., Sect. B* **30** 1904 (1974)
33. V G Tsirel'son, E V Sokolova, V S Urusov *Geokhimiya* 1170 (1986) [a]
34. J W Downs, G V Gibbs *Am. Mineral.* **72** 769 (1987)
35. J W Downs, R J Hill, M D Neuton, J A Tossel, G V Gibbs, in *Electron Distribution and Chemical Bond* (Ed. P Coppens) (New York: McGraw Hill, 1982) p. 173
36. J Lewis, in *The Xth International Congress of Crystallography (Abstracts of Reports), Amsterdam, 1975* p. 221
37. E L Belokoneva, Yu Ya Smirnitskaya, V G Tsirel'son *Zh. Neorg. Khim.* **38** 1346 (1993) [c]
38. V S Urusov, N N Eremin, O V Yakubovich *Kristallografiya* **40** 485 (1995) [d]
39. S Abrahams, E T Keve *Acta Crystallogr., Sect. A* **27** 157 (1971)
40. R J Hill, M D Newton, G V Gibbs *J. Solid State Chem.* **47** 185 (1983)
41. Yu P Dikov, I A Brytov, Yu N Romashenko *Osobennosti Elektronnogo Stroeniya Silikatov* (The Features of Electronic Structure of Silicates) (Moscow: Nauka, 1979)
42. V S Urusov *Energeticheskaya Kristallokhimiya* (Energy Crystal Chemistry) (Moscow: Nauka, 1975)
43. Yu V Ivanov, E L Belokoneva, J Protas, N K Hansen, V G Tsirelson *Acta Crystallogr., Sect. B* **54** 774 1998
44. J Protas *MOLDOS96/MOLLY, MS DOS Updated Version;* M K Hansen *SALLY MS DOS Updated Version. Unpublished. LCM3B Faculty des Sciences University Henry Poincare, Nancy* 1997
45. G V Gibbs, M A Spackman, M B Boisen *Am. Mineral.* **77** 741 (1992)
46. O A Evdokimova, E L Belokoneva, V G Tsirel'son, V S Urusov *Geokhimiya* 677 (1988) [b]
47. E L Belokoneva, V G Tsirelson *Z. Naturforsch., A Phys. Sci.* **48** 41 (1993)
48. O A Evdokimova, E L Belokoneva, V S Urusov *Zap. L'vovsk. Miner. O-va. Miner. Sb.* **43** (1) 3 (1989)
49. G Artioli, R Rinaldi, K Stahl, P F Zanazzi *Am. Mineral.* **78** 762 (1993)
50. G Artioli, R Rinaldi, C C Wilson, P F Zanazzi *Acta Crystallogr., Sect. B* **51** 733 (1995)
51. E L Belokoneva, O A Evdokimova, V G Tsirel'son, V S Urusov *Vestn. Mosk. Univ., Ser. Geologiya* 60 (1992)
52. A Hoelscher, W Schreyer *Eur. J. Mineral.* **1** 21 (1989)
53. S M Clark, G N Greaves, M Oversluzien, G Sankar, J M Thomas *International Union of Crystallography. The XYIIth Congress (Abstracts of Reports), Seattle, 1996* MS01.05.02 C-23
54. P Thomas, T Gouby, D Mercurio, T Merle, B Frit *Mat. Res. Bull.* **30** 141 (1995)
55. A A Godovikov *Mineralogiya* (Mineralogy) (Moscow: Nedra, 1983)
56. W S Fyfe *Geochemistry of Solids, An Introduction* (New York: McGraw-Hill, 1964)
57. E L Belokoneva, Yu Ya Smirnitskaya, V G Tsirel'son *Zh. Neorg. Khim.* **37** 1588 (1992) [c]
58. N V Belov, B A Maksimov, Yu Z Nozik, L A Muradyan *Dokl. Akad. Nauk. SSSR* **239** 842 (1978) [e]
59. M P C M Krijn, D Feil *Chem. Phys.* **85** 1 (1986)
60. K Olovsson, G J McIntyre, H Ptasiewicz-Bak, in *The Conference on the Charge, Spin, and Momentum Densities. Sagamore X (Abstracts of Reports), Konstanz, 1991* p. 89
61. K Hermansson *Acta Crystallogr., Sect. B* **41** 161 (1985)
62. J N Murrel, S F A Kettle, J H Tedder *Valence Theory* (New York: Wily, 1965)
63. J N Vargese, E N Maslen *Acta Crystallogr., Sect. B* **41** 184 (1985)
64. E L Belokoneva, V G Tsirel'son *Zh. Neorg. Khim.* **38** 1351 (1993) [c]
65. C S Frampton, M-A Rennie, P R Raithby *Bull. Czech. Slovak Crystallogr. Assoc., (Spec. Issue A, ECM18)* **5** 12 (1998)
66. P J MacDougal, M B Hall, R F W Bader, J R Cheeseman *Can. J. Chem.* **67** 1842 (1989)
67. R J Gillespie, J Butheway, T-H Tang, R F W Bader *Inorg. Chem.* **35** 3954 (1996)
68. D K Swanson, C T Prewitt *Am. Mineral.* **68** 581 (1983)
69. S Sasaki, Y Takeuchi, K Fujino, S Akimoto *Z. Kristallogr.* **158** 279 (1982)
70. Y Takeuchi, Y Kudoh *Z. Kristallogr.* **146** 281 (1977)
71. R C Peterson Ph D Thesis, Virginia Polytechnical Institute, University of Blacksburg, Virginia, 1980
72. E L Belokoneva, A N Goryunova *Zh. Neorg. Khim.* **42** 2050 (1998) [c]

73. V A Strel'tsov, V E Zavodnik *Kristallografiya* **34** 1369 (1989) [d]
74. A C Hess, V R Saunders *J. Phys. Chem.* **96** 4367 (1992)
75. L Benco, L Smrcok *Phys. Chem. Miner.* **21** 401 (1994)
76. L Smrcok, L Benco *Am. Mineral.* **81** 1405 (1996)
77. L Benco, L Smrcok *Eur. J. Mineral.* **10** 483 (1998)
78. R Dovesi, C Pisani, C Roetti, M Causa, V R Saunders *CRYSTAL92. Ab initio Electron LCAO-Hartree-Fock Program for Periodic Systems, Indiana University, Bloomington, IN, 1992*
79. R F Stewart, W A Whitehead, G Donnay *Am. Mineral.* **65** 324 (1980)
80. N Thron, D Schwarzenbach, in *The European Crystallography Meeting (Abstracts of Reports), Copenhagen, 1979* p. 348
81. K L Geisinger, M A Spackman, G V Gibbs *J. Phys. Chem.* **91** 3237 (1987)
82. J W Downs *J. Phys. Chem.* **99** 6849 (1995)
83. R D Shannon, C T Prewitt *Acta Crystallogr., Sect. B* **25** 925 (1969)
84. J W Downs, R J Swope *J. Phys. Chem.* **96** 4834 (1992)
85. E Stuckenschmidt, W Joswig, W H Baur *Phys. Chem. Miner.* **19** 562 (1993)
86. E Stuckenschmidt, W Joswig, W H Baur *Phys. Chem. Miner.* **21** 309 (1994)
87. N E Ghermani, C Lecompte, Y Dusausoy *Phys. Rev. B Condens. Matter* **53** 5231 (1996)
88. Yu V Ivanov, E L Belokoneva, J W Downs, V G Tsirel'son *Kristallografiya* (1999) (in the press) [d]
89. J C White, A C Hess *J. Phys. Chem.* **97** 6398 (1993)
90. M B Boisen Jr , G V Gibbs, M S T Bukowinski *Phys. Chem. Miner.* **21** 269 (1994)
91. G V Gibbs, F C Hill, M B Boisen Jr *Phys. Chem. Miner.* **24** 167 (1997)
92. R Nada, C R A Catlow, R Dovesi, V R Saunders *Proc. R. Soc. Lond., A, Math. Phys. Sci.* **436** 499 (1992)
93. Ph D Arco, G Sandrone, R Dovesi, E Apra, V R Saunders *Phys. Chem. Miner.* **21** 285 (1994)
94. R E Cohen *Am. Mineral.* **76** 733 (1991)
95. D M Sherman *J. Geophys. Res.* **98** 11865 (1993)
96. R J Hill, M D Newton, G V Gibbs *J. Solid State Chem.* **47** 185 (1983)
97. M A Spackman, R J Hill, G V Gibbs *Phys. Chem. Miner.* **14** 139 (1987)

[a] — *J. Struct. Chem. (Engl. Transl)*
[b] — *Geochem. Int. (Engl. Transl.)*
[c] — *Russ. J. Inorg. Chem. (Engl. Transl.)*
[d] — *Russ. Crystallogr. (Engl. Transl.)*
[e] — *Dokl. Chem. Technol., Dokl. Chem. (Engl. Transl.)*